



Process-oriented assessment of RCA4 regional climate model projections over the Congo Basin under 1.5 °C and 2 °C global warming levels: influence of regional moisture fluxes

Alain T. Tamoffo^{1,2} · Wilfran Moufouma-Okia³ · Alessandro Dosio⁴ · Rachel James⁵ · Wilfried M. Pokam^{1,2,6} · Derbetini A. Vondou^{1,2} · Thierry C. Fotso-Nguemo^{1,7} · Guy Merlin Guenang^{1,8} · Pierre H. Kamsu-Tamo^{1,9,10} · Grigory Nikulin¹¹ · Georges-Noel Longandjo¹² · Christopher J. Lennard¹³ · Jean-Pierre Bell¹⁴ · Roland R. Takong¹³ · Andreas Haensler¹⁵ · Lucie A. Djotchou¹ · Robert Nouayou¹⁶

Received: 30 August 2018 / Accepted: 28 March 2019 / Published online: 6 April 2019
© Springer-Verlag GmbH Germany, part of Springer Nature 2019

Abstract

Understanding the processes responsible for precipitation and its future change is important to develop plausible and sustainable climate change adaptation strategies, especially in regions with few available observed data like Congo Basin (CB). This paper investigates the atmospheric circulation processes associated with climate model biases in CB rainfall, and explores drivers of projected rainfall changes. Here we use an ensemble of simulations from the Swedish Regional Climate Model (RCM) RCA4, driven by eight General Circulation Models (GCMs) from the Coupled Model Intercomparison Project Phase 5 (CMIP5), for the 1.5 °C and 2 °C global warming levels (GWLS), and under the representative concentration pathways (RCPs) 4.5 and 8.5. RCA4 captures reasonably well the observed patterns of CB rainfall seasonality, but shows dry biases independent of seasons and large scale driving atmospheric conditions. While simulations mimic observed peaks in transition seasons (March–May and September–November), the rain-belt is misplaced southward (northward) in December–February (June–August), reducing the latitudinal extent of rainfall. Moreover, ERA-Interim reanalysis driven RCM simulation and RCM–GCM combinations show similar results, indicating the dominance of systematic biases. Modelled dry biases are associated with dry upper-tropospheric layers, resulting from a western outflow stronger than the eastern inflow and related to the northern component of African Easterly Jet. From the analysis of the climate change signal, we found that regional scale responses to anthropogenic forcings vary across GWLS and seasons. Changes of rainfall and moisture divergence are correlated, with values higher in March–May than in September–November, and larger for global warming of 2.0 °C than at 1.5 °C. There is an increase of zonal moisture divergence fluxes in upper atmospheric layers (> 700 hPa) under RCP8.5 compared to RCP4.5. Moreover, it is found that additional warming of 0.5 °C will change the hydrological cycle and water availability in the CB, with potential to cause challenges to water resource management, agriculture, hydro-power generation, sanitation and ecosystems.

Keywords Congo Basin rainfall biases · RCA4 · CMIP5 · Moisture convergence · Global warming levels · RCPs

1 Introduction

The global response to the threat of climate change has been strengthened in recent years with the adoption of the Paris climate Agreement's ambitious long-term goal to holding the increase of global average temperature to well below 2 °C above pre-industrial levels and pursuing efforts to limit the temperature increase to 1.5 °C above pre-industrial levels. The Agreement invited the Intergovernmental Panel on Climate Change (IPCC) to produce a Special Report detailing impacts of global warming of 1.5 °C above pre-industrial

Electronic supplementary material The online version of this article (<https://doi.org/10.1007/s00382-019-04751-y>) contains supplementary material, which is available to authorized users.

✉ Alain T. Tamoffo
alaintamoffotchio@gmail.com

Extended author information available on the last page of the article

levels and related global greenhouse gas emission pathways (Masson-Delmotte et al. 2018). This special report indicates that climate-related risks for natural and human systems depend on the magnitude of global warming, geographic location, level of development, vulnerability, choices and implementation of adaptation and mitigation options; recognizing the growing needs for solution-focused and spatially detailed climate information.

To this regard, an improved understanding of the geo-physical mechanisms underpinning climate-related impacts and risks to humans and natural systems especially at 1.5 °C and 2 °C global warming levels (GWLs) is critical, specifically over the Congo Basin (CB)—a vulnerable region in which multiple biophysical, political, and socioeconomic stresses interact to constrain the adaptive capacity, and where the economy strongly depends on climate sensitive sectors including rain-fed agriculture, forestry, hydro-electricity, breeding and water resource management (IPCC 2007; Masson-Delmotte et al. 2018; King and Harrington 2018). The CB plays a pivotal role in the climate system, being one of the three most convective regions on the planet (Washington et al. 2013). The region also encompasses the largest river basin in Africa and the Congo rainforest, acting as the planet's second largest lung after the Amazon rainforest (Baccini et al. 2012; Fisher et al. 2013; Dargie et al. 2017). Yet, the drivers of the regional climate of the CB remain largely understudied due to the dearth of observational data (Williams et al. 2007; Jury et al. 2009; Baccini et al. 2012; Fisher et al. 2013; Zhang et al. 2013; Panitz et al. 2014).

The vertically integrated moisture flux is an important mechanism of the hydrological cycle in CB and helps connecting precipitation to large-scale atmospheric circulation systems (Pokam et al. 2012). Precipitation originates from water balance components: moisture already contained in the atmosphere, remote moisture transport and from local evaporation of surface moisture by recycling fallen precipitation (Van der Ent et al. 2010; Van der Ent and Savenije 2013; Dyer et al. 2017). Moisture flux, through complex feedback mechanisms, determine the rainfall amount and is linked to dry or wet conditions (Muller et al. 2009; Washington et al. 2013; Yin et al. 2013; Shi et al. 2014). General circulation models (GCMs) often show dry (wet) biases related to strong moisture divergence (convergence) outward (inward) to the region (Washington et al. 2013). Creese and Washington (2016) demonstrated a strong positive correlation between precipitation and moisture flux convergence at 700 hPa in March–May (MAM), and at 850 hPa in June–November (JJASN) and December–February (DJF). Moisture flux convergence peaks during the MAM and SON rainy seasons (Washington et al. 2013). However, there are large uncertainties on the dominant moisture sources in the lower troposphere. A divergent circulation from Atlantic

Ocean toward the inland is generally cited as the important source of moisture (Nicholson and Grist 2003; Dezfuli and Nicholson 2013; Pokam et al. 2014; Dezfuli et al. 2015). In contrast, other investigations indicate the Indian Ocean as dominant moisture source (Van der Ent et al. 2010; Van der Ent and Savenije 2013; Dyer et al. 2017). There is rather an agreement in identifying the north branch of African easterly jet (AEJ-N) as upper layer moisture sources, stronger in MAM relative to SON (Pokam et al. 2012; Washington et al. 2013; Dyer et al. 2017).

GCMs are the primary tools for making climate projections and exploring large-scale responses of the climate system to various forcings (Qin et al. 2013). However, their coarse grid spacing poses serious challenges to capture mesoscales processes and phenomena in Africa including organised convection, land–atmosphere interactions, sharp gradients in temperature, soil moisture, potential vorticity, influence of lakes, mountain ranges, weather fronts (Cook 1999; Koster et al. 2004; Jackson et al. 2009; Taylor et al. 2012; Washington et al. 2013; Watterson et al. 2014; Birch et al. 2014; Aloysius et al. 2016; Creese and Washington 2018; Gibba et al. 2018; James et al. 2018; Sonkoué et al. 2018). The influences from ocean basins, prominent modes of natural variability, and aerosol emissions add extra layers of complexity to be accounted for (Rowell 2013; Giannini et al. 2008).

A key gap in the provision of credible regional climate change information is the mismatch between GCM's scale and the spatial scale needed for vulnerability and impact applications. Dynamical downscaling methods based on high-resolution regional climate models (RCMs) are designed to better capture smaller scale physiographic processes (Laprise 2008; Rowell 2013; Giorgi and Gutowski 2015; Moufouma-Okia and Jones 2015). RCMs have been widely applied across Africa in the framework of CORDEX (the COordinated Regional climate Downscaling EXperiment; Giorgi et al. 2009), an international research effort of World Climate Research program (WCRP, <http://www.wcrp-climate.org/>) to sample uncertainties from ensembles of spatially detailed historical and future climate projections of regional climate for all land regions of the globe—through downscaling of GCMs from the Coupled Model Intercomparison Projects Phase 5 (CMIP5; Taylor et al. 2012). CORDEX has shown substantial progress in assessing model simulations of precipitation characteristics over Africa, and indicated the added value of RCMs relative to driving GCMs and reanalyses (Tchotchou and Kamga 2010; Nikulin et al. 2012; Laprise et al. 2013; Kim et al. 2014; Panitz et al. 2014; Dosio and Panitz 2016; Fotso-Nguemo et al. 2017; Gibba et al. 2018). However, some precipitation biases exist and remain less understood (Diallo et al. 2012; Kalognomou et al. 2013; Paeth and Mannig 2013; Diaconescu and Laprise 2013; Haensler et al. 2013; James et al.

2013; Kim et al. 2014; Gboganiyi et al. 2014; Panitz et al. 2014; Crétat et al. 2014; Lee and Hong 2014; Giorgi et al. 2014; Watterson et al. 2014; Dosio and Panitz 2016; Fotso-Nguemo et al. 2016; Vondou and Haensler 2017; Tamoffo et al. 2019).

The prerequisite to applying climate models for credible future projections is the model systematic evaluation through comparisons against observations. Model performance is commonly assessed by comparing simulated local, regional and large-scale climate quantities with corresponding observationally based estimates and using quantitative statistical measures, referred to as “performance metrics” including root mean square error, pattern correlation coefficient, standard deviation (Flato et al. 2013; Rowell 2013). Reproducing such metrics is a critical “reality” check for climate models. While performance metrics are useful instruments to identify large-scale problems and simplify the visualization of model performance, they provide limited information about causes and ways to address the issues (Gleckler et al. 2008; Nishii et al. 2012).

Several recent studies have therefore recommended the use of a “process-based” approach instead of performance metrics to evaluate climate models’ performance over Africa, with view to further understand the models’ ability to simulate processes on a regional scale (Roehrig et al. 2013; Washington et al. 2013; Creese and Washington 2016, 2018; James et al. 2018; Howard and Washington 2018). This is fundamental to determine ways to improve models’ performance, and a prerequisite to assess models’ adequacy for future projection (James et al. 2015; Rowell et al. 2016; Baumberger et al. 2017).

In this study, we apply for the first time a process-based assessment approach to an ensemble of transient RCM simulations from the Rossby Centre RCM (RCA4) over the Congo Basin, following the work of Creese and Washington (2016). The purpose of the article is twofold: first, we investigate the interlinkages between simulated regional atmospheric circulations and rainfall biases, with view to provide avenues for improving model’s representation of key physical and regional processes. Second, we explore the influence of moisture fluxes in modulating projected hydrological changes under the 1.5 °C and 2 °C global warming levels. Through examination of moisture flux changes, we hope to foster the understanding physical mechanisms underpinning future changes and assess their plausibility, as well as to simulate discussions about the challenges and opportunities of process-based assessment of RCM in equatorial Africa.

The paper’s outline is as follows. In Sect. 2, we provide a brief description of the RCA4 regional climate model, experimental configuration, validation data and key metrics used. Section 3 evaluates the baseline climatological features of simulated precipitation in the Congo Basin region. Section 4 examines regional atmospheric circulations and their

interlinkages with simulated precipitation biases. Section 5 focuses on projected moisture changes. Section 6 discusses key findings and provides a summary.

2 Methodology

2.1 Regional climate model and experimental design

This study uses the latest version of the regional climate model RCA4 developed by the Swedish Rossby Center (Samuelsson et al. 2011). RCA4 originates from the numerical weather prediction model HIRLAM (Unden et al. 2002), with improved physical and dynamical parameterizations (Strandberg et al. 2015). It employs a quadrilled land-surface scheme (LSS) with one to three key tiles as recommended by land-use information. The convection scheme is that of Kain–Fritsch (Kain 2004) and supposes that shallow convection is non-precipitating. The radiation scheme gets from HIRAM’s radiation scheme (Savijärvi 1990; Sass et al. 1994) and modified after Räisänen et al. (2000), aiming to take into account the carbon dioxide absorption and an improved treatment of the water vapor cycle. The vegetation-dependent land-surface parameters is applied after Noilhan and Planton (1989). Six-order linear horizontal diffusion, associated to two time-level, semi-lagrangian and semi implicit scheme are applied to the prognostic variables (Jones et al. 2004). Refer to Strandberg et al. (2015) for full details about main changes in RCA3 to achieve RCA4.

Several RCA4 simulations were performed over the CORDEX-Africa domain, with a 0.44° horizontal resolution (~ 50 km). First, the model was integrated from January 1979 through December 2010 in a quasi-perfect forcing mode, using lateral and initial boundary conditions from the ERA-Interim reanalysis. Second, RCA4 was integrated from January 1950 through December 2100 to downscale eight CMIP5 GCMs (see list and details in Table 1). Historical simulations are driven by observed natural and anthropogenic atmospheric composition, and available from 1950 to 2005, while climate projections run from 2006 to 2100 under Representative Concentration Pathways (RCPs) 4.5 and 8.5 scenarios (Thomson et al. 2011; Riahi et al. 2011; Samuelsson et al. 2015). The availability of RCA4’s transient historical and future climate simulations nested within multiple GCMs, in the framework of CORDEX, offers the possibility to elucidate the regional model’s response of moisture flux changes to various forcings and GWLs over CB.

Model validation is carried out through comparing RCM historical and quasi-perfect simulations against observational and reanalysis datasets (see list and details in Table 2), thus accounting for the observational uncertainty (Vondou and Haensler 2017). Due to the low spatial

coverage of in-situ stations over CB, observed data are obtained from various methods of deriving total precipitation in the region by mixing different sources of data such as station measurements, reanalysis products and satellite estimates. To facilitate the comparison, all observational and reanalysis products have been remapped to match the simulation grids as follows: all data with native resolution less than 0.44° are re-gridded into the reference grid using the first order conservative remapping method (Jones 1999), while those with analogous or coarser resolution than 0.44° are interpolated through bilinear interpolation (Nikulin et al. 2012).

2.2 Definition of GWLs

There are several approaches to determine regional climate responses associated with GWLs (James et al. 2017). In this paper, the 1.5°C and 2°C responses are extracted from transient experiments by selecting time samples at the date when the 30-year running mean global temperature reaches 1.5°C or 2°C compared to a control period (CTL), 1971–2000. A list of RCM–GCM combinations and the future 30-year periods of GWLs 1.5°C and 2.0°C were computed as described in (Nikulin et al. 2018) and are given in Table 3. As stated by (Nikulin et al. 2018), the period 1971–2000 is a frequently selected as baseline time slice for impact application investigations and consistent with previous GWL

Table 1 List of driving CMIP5 GCMs used in this study

Model name	Institution	Native resolution	References
CanESM2	Canadian Centre for Climate Modelling and Analysis	$2.8^\circ \times 2.8^\circ$	Chylek et al. (2011)
CNRM-CM5	National Center for Meteorological Research/European	$1.4^\circ \times 1.4^\circ$	Volodko et al. (2013)
EC-EARTH-ES	European community Earth-System Model Consortium	$1.125^\circ \times 1.125^\circ$	Hazeleger et al. (2010)
HadGEM2-ES	Met Office Hadley Centre	$1.875^\circ \times 1.25^\circ$	Collins et al. (2011)
IPSL-CM5A-MR	Institut Pierre-Simon Laplace	$2.5^\circ \times 2.5^\circ$	Dufresne et al. (2013)
MIROC5	Atmosphere and Ocean Research Institute (University of Tokyo)	$1.40^\circ \times 1.40^\circ$	Watanabe et al. (2011)
MPI-ESM-LR	Max Planck Institute for Meteorology	$1.9^\circ \times 1.9^\circ$	Popke et al. (2013)
NorESM1-M	Norwegian Climate centre	$2.5^\circ \times 1.9^\circ$	Bentsen et al. (2013)

Table 2 List of observational or reanalysis products used in this study

Datasets	Institution	Native resolution	References
GPCC	Global Precipitation Climatology Centre	$0.5^\circ \times 0.5^\circ$	Schneider (2011)
CMAP	Climate Prediction Centre (CPC) Merged Analysis of Precipitation, NOAA NCEP	$2.5^\circ \times 2.5^\circ$	Xie and Arkin (1997)
CRU	Climate Research Unit, University of East Anglia (v4.01)	$0.5^\circ \times 0.5^\circ$	Harris et al. (2014)
GPCP	Global Precipitation Climatology Project,	$2.5^\circ \times 2.5^\circ$	Huffman et al. (2009)
ERA-Interim	European Centre for Medium Range Weather Forecasts	$0.75^\circ \times 0.75^\circ$	Dee et al. (2011)
NCEP-I-II	National Centers for Environmental	$2.5^\circ \times 2.5^\circ$	Kalnay et al. (1996)– Kanamitsu et al. (2002)

Table 3 Timing of 30-year period of targeted GWLs as a function of RCPs and corresponding driving GCM

Model name	Member	Version	RCP4.5		RCP8.5	
			+ 1.5°C	+ 2.0°C	+ 1.5°C	+ 2.0°C
CanESM2	r1i1p1	v1	2002–2031	2017–2046	1999–2028	2012–2041
CNRM-CM5	r1i1p1	v1	2021–2050	2042–2071	2015–2044	2029–2058
EC-EARTH-ES	r12i1p1	v1	2010–2039	2031–2060	2005–2034	2021–2050
HadGEM2-ES	r1i1p1	v2	2016–2045	2032–2061	2010–2039	2023–2052
IPSL-CM5A-MR	r1i1p1	v1	2002–2031	2020–2049	2002–2031	2016–2045
MIROC5	r1i1p1	v1	2026–2055	2059–2088	2019–2048	2034–2063
MPI-ESM-LR	r1i1p1	v1	2006–2035	2029–2058	2004–2033	2021–2050
NorESM1-M	r1i1p1	v1	2027–2056	2062–2091	2019–2048	2034–2063

studies in Africa. The timing for GWLs in the GCMs is very variable, demonstrating the model-dependent responses of the climate system to anthropogenic forcings. The time/year when a GCM reaches a fixed GWL is a function of the GCM–RCP combination, due to a different climate sensitivities in the GCM (Teichmann et al. 2018). To investigate the influence of 1.5 °C versus 2.0 °C, the differences in impact were compared by plotting separately each model runs (see supporting information) and the ensemble-mean change at one warming level versus CTL for each grid point. The difference in effects of the two GWLs was also evaluated under the RCP4.5 and RCP8.5. The climate change signals are obtained through the differences of mean value between the future and the CTL, considering the two GWLs.

2.3 Estimating the moisture flux convergence

The total content of atmospheric moisture column has been estimated using the water budget equation from Newell et al. (1972), expressed as follows:

$$\frac{dW}{dt} - (-\nabla \cdot Q) = E - P \quad (1)$$

The term $\frac{dW}{dt} = \frac{d}{dt}(\frac{1}{g} \int_{P_{bot}}^{P_{top}} q dp)$ of this equation, denotes variations of precipitable water in the atmospheric column; $-\nabla \cdot Q$ represents moisture flux convergence; E is evaporation; and P precipitation. q is specific humidity (in g/kg); g is intensity of gravity (in N/kg); P_{bot} is surface pressure and P_{top} pressure of top level (in N m⁻²). On non-synoptic time scale, the storage of water vapor is steadfastness (i.e. $\frac{dW}{dt} = 0$, Trenberth 1999; Seneviratne et al. 2004). Thus Eq. (1) can be approximately written as follows:

$$\nabla \cdot Q = E - P \quad (2)$$

To estimate the term Q, we split it in their zonal (Q_λ) and meridional (Q_ϕ) components expressed as follows (Zheng and Eltahir 1998):

$$Q_\lambda = \frac{1}{g} \int_{P_{bot}}^{P_{top}} u q dp \quad \text{and} \quad Q_\phi = \frac{1}{g} \int_{P_{bot}}^{P_{top}} v q dp \quad (3)$$

where u and v are zonal and meridional wind components respectively (in m/s). The net moisture flux convergence (divergence) is the total inflow to (outflow from) the region, scaled by the surface area. In this study it's obtained using Zheng and Eltahir (1998) method: in a given rectangular ($L \times H$) region which the atmospheric water vapor inflows and outflows, the inflow comes from the contribution of the East–West (Q_λ in kg s⁻¹) and North–South (Q_ϕ in Kg s⁻¹) boundaries. By using Gauss's theorem, the total zonal and

meridional moisture flux convergence or divergence are obtained on the time series as follows:

$$Q_\lambda = \frac{Q_{West} - Q_{East}}{S} \quad \text{and} \quad Q_\phi = \frac{Q_{South} - Q_{North}}{S} \quad (4)$$

Spatially, the total moisture convergence is given by:

$$-\nabla \cdot Q = -1 \left(\frac{dQ_\lambda}{dx} + \frac{Q_\phi}{dy} \right) \quad (5)$$

S (in m²) is surface area of the region calculated as:

$$S = R^2 \Delta\lambda (\sin\phi_2 - \sin\phi_1) \quad (6)$$

$\Delta\lambda = \lambda_2 - \lambda_1$, where λ_1 and λ_2 are respectively western (10°E) and eastern (35°E) boundary longitudes, ϕ_1 and ϕ_2 are respectively southern (10°S) and northern (10°N) boundary latitudes (all converted in radians) and R (in m) is the earth's radius. To apply this formula to gridded data, the targeted region is considered as the sum of several squares with segments length $\Delta\lambda$ in the zonal direction and $\Delta\phi$ in the meridional calculated as:

$$\Delta\lambda = \Delta\phi = 0.44 \times \frac{\pi}{180} \times R \quad (7)$$

Since 0.44° is the spatial resolution of datasets in the two directions. If N (M) is the total number of grid points in the zonal (meridional) direction, the domain size is simply obtained as follows:

$$S = L \times H = N \Delta\lambda \times M \Delta\phi \quad (8)$$

Q_{West} , Q_{East} , Q_{South} and Q_{North} are transient moisture across the respective boundary. Defined in this way, negative values indicate moisture divergence and positive values are convergence.

3 Baseline understanding of model performance

3.1 Rainfall intra-seasonal variability

Simulated intra-seasonal variabilities of CB rainfall from overall RCM runs are compared to the GPCC, CMAP, CRU, GPCP, ERA-I, NCEP 1 and NCEP 2 datasets as seen in Fig. 1a. In order to appreciate intensity gaps between simulations and observations, the natural variability contained in the observed climate is also shown through the standard deviation (shade light-blue band), from GPCC, CMAP, CRU and GPCP datasets. For a given month, a mean rainfall value greater than the corresponding standard deviation is considered as a clear failing of the considered experiment. Even though observations and reanalyses are consistent on the shape of the variability and on the bimodal characteristic

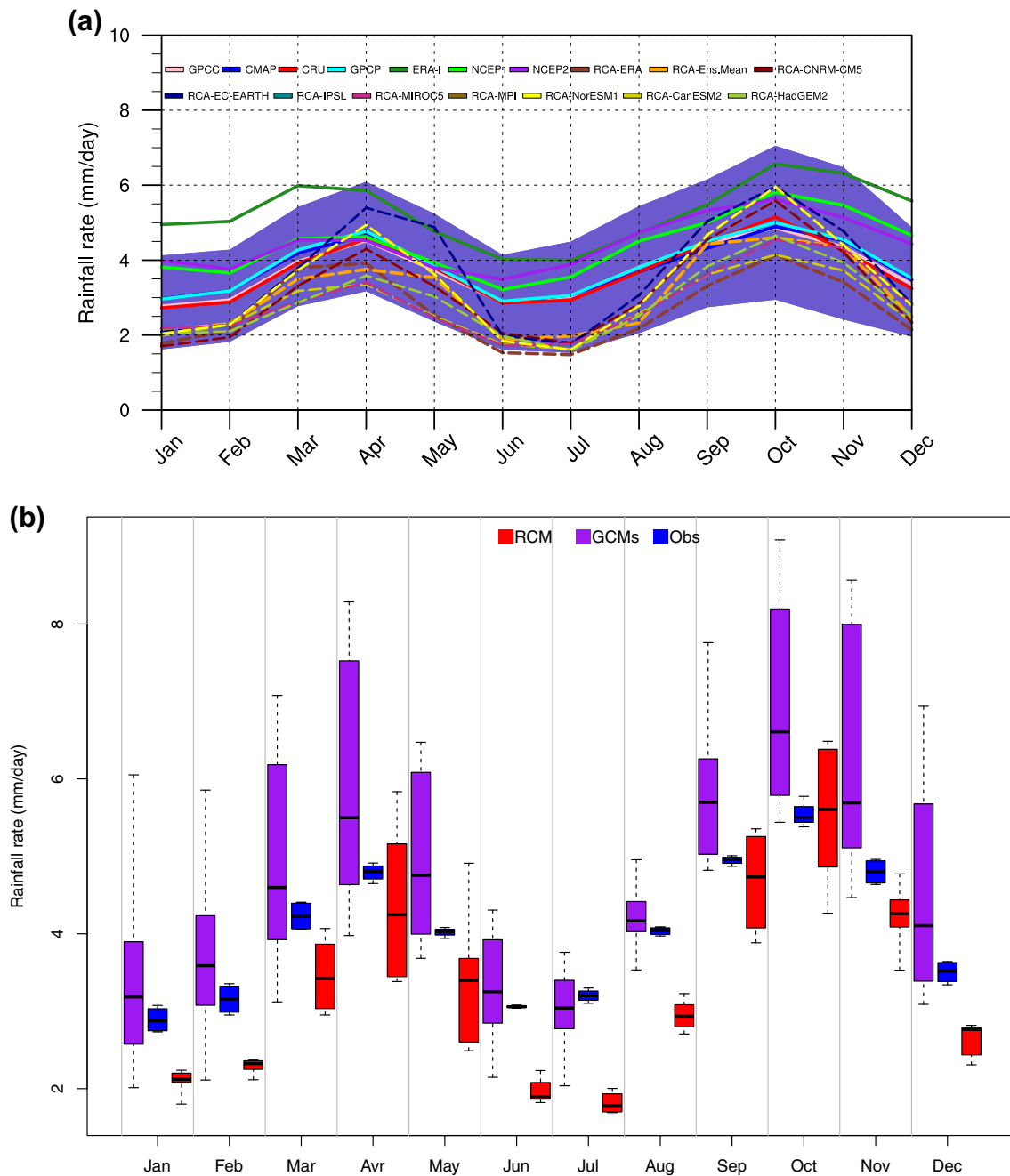


Fig. 1 **a** The 23 year mean rainfall (mm/day) for individual RCA4 runs, observations, and reanalysis data for 1983–2005. The shade light-blue band is the standard deviation and uses GPCC, CMAP,

CRU and GPCP ensemble mean. **b** Uncertainty ranges in CB rainfall (mm/day) from RCA4 runs (red), Corresponding driving GCMs (purple) and observations (blue)

of CB precipitation, with occurrence of peaks in MAM and SON transition seasons, there are differences in their magnitudes. ERA-I features the highest rate rainfall with maximums peaking in March and October.

Although RCM runs reproduce well basic patterns of seasonal cycle and well depict the wetter character of SON relative to MAM (Washington et al. 2013), there is a crucial issue in their simulations of rainfall magnitudes. Two runs

overvalue the MAM peak in April (RCA-EC-EARTH and RCA-NorESM1); one in March (RCA-EC-EARTH) whilst the rest of experiments underestimate. In the wettest season SON, experiments tend to divide into two groups: five drier runs (RCA-ERA, RCA-HadGEM2, RCA-MIROC5, RCA-CanESM2, RCA-IPSL) with peaks less than 4.5 mm/day and four wetter runs (RCA-EC-EARTH, RCA-NorESM1, RCA-CNRM-CM5, RCA-MPI) with peaks greater than

4.5 mm/day. In dry seasons (DJF and JJA), all simulations strongly underestimate rainfall rates, with difference between the wettest and driest up to 1.5 mm/day. However, the JJA minimum rate of rainfall is weaker than that of DJF. This result has been likewise reported by Washington et al. (2013) and Creese and Washington (2016).

In Fig. 1b the ranges from the observations (GPCC, CMAP, CRU and GPCP) and RCA4 runs are compared to the global driving models. This has helped to highlight the presence of largest uncertainty rates in simulated rainy seasons precipitation in CMIP5 driving datasets, and that these uncertainties decrease during the downscaling process. Moreover, comparing uncertainty ranges of RCM runs to those of driven GCMs, it emerges that the regional signal strongly influences boundary conditions from driven GCMs. For a better understanding of downscaling effects, an analysis of rainfall spatial distribution must be done.

3.2 Quantification of rainfall pattern similarities

The comparison of modeled seasonal spatial patterns of mean rainfall by RCA-EnsMean and RCA-ERA with GPCC, CMAP, CRU, GPCP, ERA-I, NCEP1 and NCEP2 observational and reanalysis datasets is depicted in Fig. 2. Model's rainfall biases relative to GPCP are shown in Fig. 3. Also see figures S1 and S2 in the supporting information for individual RCA4 outputs of mean precipitation climatology and rainfall' biases respectively, and figure S3 for corresponding driving GCMs rainfall' biases.

The alternation of wet and dry seasons over CB is generally assigned to the northward and southward excursions of the Inter-Tropical Convergence Zone [ITCZ, Nicholson and Grist (2003) and Jackson et al. (2009)], although Nicholson (2018) highlights that the rainfall maximum does not collocate with surface convergence. Nevertheless, one of challenges in modelling of region's rainfall is to reproduce that observed seasonality. In general, simulations capture well the basic pattern of rainfall variability and succeed the spreading of western rainfall maxima, which focus on the Atlantic coast and over the Gulf of Guinea (Figs. 2 and S1). They show an almost similar structure of spatial rainfall distribution. However, some biases are still evident: all RCA4 setups produce a weaker rainfall magnitude over major part of CB region and for all seasons (Figs 3 and S2). In dry season DJF (JJA), the rain-belt is misplaced further southward (northward) in all experiments than in observation datasets. This implies a reduction of the latitudinal extent of the rainfall band (see columns 1 and 3 in Figs 2 and S1). In MAM and SON, the driest experiments have much less rainfall over Democratic Republic of Congo. In particular, for MAM, they show a northern and southern rainfall minimum; some of them, e.g. RCA-HadGEM2, also show an eastern rainfall

minimum; in SON, all experiments heralds rather a tendency to overestimate (underestimate) southern (eastern) rainfall.

To distinct the model "structural bias" with combined effects of this last and LBC errors, RCA4 forced by ERA-Interim (RCA-ERA), the ensemble means of all GCM forcings (RCA-EnsMean) and from corresponding driving GCMs (EnsMean) have been analysed (Fig 3). It follows that the RCA-ERA "evaluation" simulation is closer to downscaled GCMs than observations; the RCA-EnsMean is similar to most of individual RCM runs added to a common dry bias in all experiments over a major area of CB region (Fig S2). Yet, "structural biases" of driving GCMs (Fig S3) are not alike to that of corresponding RCM runs. For instance, GCMs' ensemble mean (EnsMean, row 3 in Fig 3) shows wet biases in MAM and SON and slight dry biases in DJF and JJA. However, the ensemble mean of RCM runs (RCA-EnsMean, row 2 in Fig 3) displays stronger dry biases, independently of seasons. These findings indicate that RCA4 internal processes play a dominant role in determining model wetness or dryness.

Taylor diagrams are used to summarize the spatiotemporal differences or similarities between observed and simulated fields (Fig 4). The Taylor diagram displays three statistical measures with respect to one reference field. The distance between reference and individual points in the Taylor diagram (black circles) corresponds to root-mean-square difference (RMSD). The black radial lines display the pattern correlation (r) between the simulated and the reference field. The black dotted circles represent the spatial standard deviation (STD) between the simulated and the reference field.

Results shown are based on the interannual variation of seasonal (DJF, MAM, JJA and SON) mean precipitation for the current climate. Each model run is evaluated with respect to the reference field (GPCP). RCA4 outputs and their ensemble mean (RCA-Ens.Mean) have been compared with the observed dataset. To supply an overview of observational uncertainty over the CB, GPCC, CRU, PRECL, NCEP-1,2 and ERA-I are also contrasted to GPCP and shown on the common diagram. For all seasons, station measures (GPCC, CRU, PREC-L) are more clustered and close to the reference field with best performances (RMSD < 0.5; $r \sim 0.95 + / - 0.05$; and STD $\sim 1 + / - 0.25$). This better consistency between observations is expected, since the three products are sharing most of the meteorological stations rainfall data for gridding. There are inconsistent and less performances of reanalyses (NCEP-1,2, ERA-I) compared to station measurements with $r \sim 0.85 + / - 0.02$; RMSD $\sim 0.65 + / - 0.15$ and STD $\sim 1.25 + / - 0.25$. Skills of the simulations in reproducing rainfall varies unremarkably according to the data used to force the model. r values are within the range $0.58 + / - 0.25$, RMSD $\sim 1.15 + / - 0.55$ and STD $\sim 1.40 + / - 0.40$. RCA-EnsMean tends to

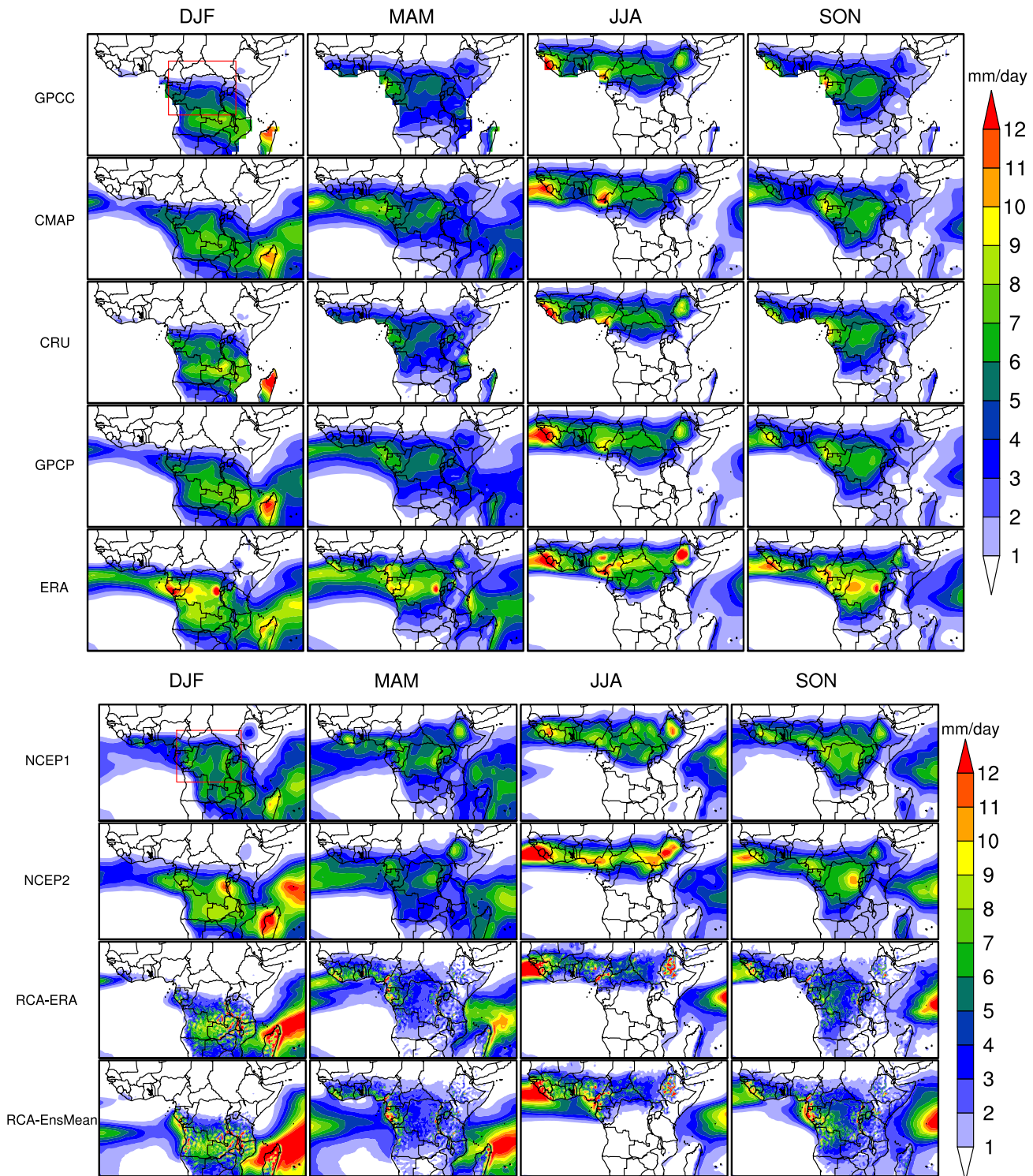


Fig. 2 Mean (1983–2005) seasonal rainfall (mm/day) for DJF (column 1), MAM (column 2), JJA (column 3) and SON (column 4), for the “evaluation” run (RCA-ERA); the ensemble mean of RCA4-runs (RCA-EnsMean) and from reanalysis and observational products. See names of datasets left of panel. The red box delimits the CB region as defined in this study

outperform individual simulations in rainy seasons. For all seasons, RCA-ERA's statistical parameters are closer to those of RCM-runs than observational or reanalyses. This

confirms that boundary condition effects are negligible relative to the model physics (Diallo et al. 2016). Thus, model's errors over the CB region are systematic biases.

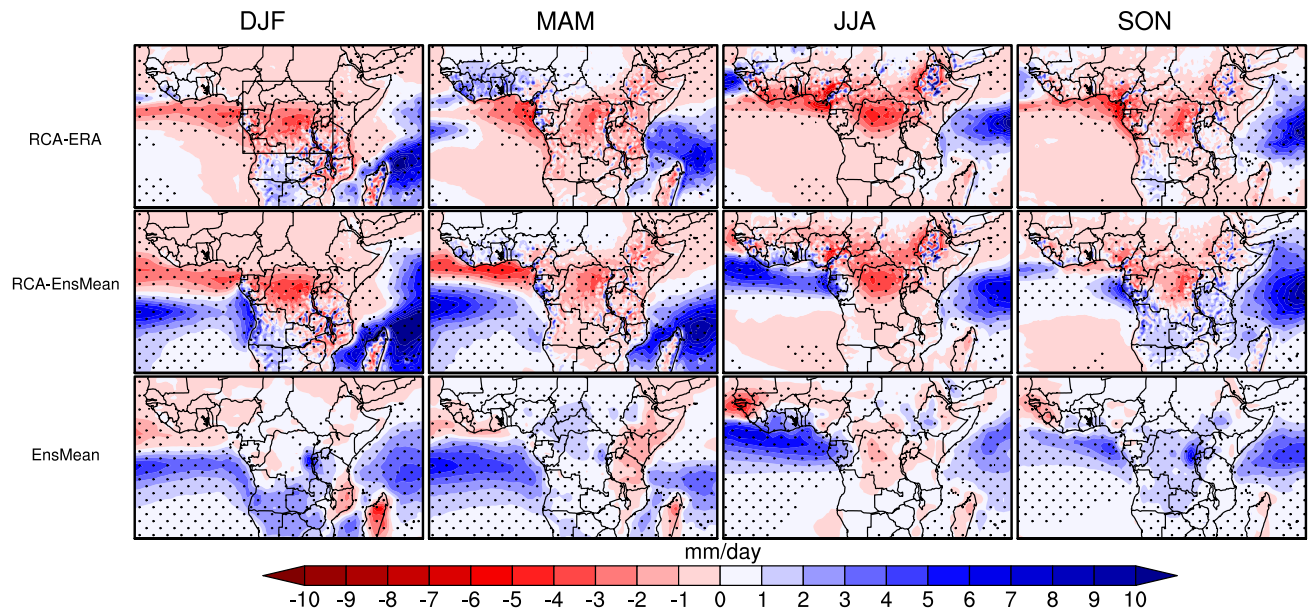


Fig. 3 Mean rainfall biases (mm/day) for DJF (column 1), MAM (column 2), JJA (column 3) and SON (column 4), for the “evaluation” run (RCA-ERA; row 1), from the ensemble mean of RCA4-runs (RCA-EnsMean; row 2) and from ensemble mean of driving GCMs

(EnsMean; row 3). Stippling indicates 95% significance level using t-test. See names of different datasets left of panel. The black box delimits the CB region as defined in this study

4 Potential causes for rainfall biases

4.1 Moisture flux convergence

In order to understand causes of modeled dry biases over the CB region, we have first focused our attention on the simulated upstream moisture flux convergence. The moisture flux dynamic and its contribution to the CB rainfall has already been analyzed by some studies (Van der Ent et al. 2010; Van der Ent and Savenije 2013; Pokam et al. 2012, 2014; Washington et al. 2013; Creese and Washington 2016; Dyer et al. 2017). They have helped to establish that the credibility of a model to simulate rainfall is positively correlated to its ability to reproduce correctly moisture flux climatology, especially for tropical regions where moisture flux convergence strongly modulates the hydrological cycle (Pokam et al. 2012).

The intra-seasonal variability of moisture flux convergence across atmospheric layers is shown in Fig. 5. RCA-ERA and RCA-EnsMean experiments are compared to three reanalysis products NCEP 1 (row 1), NCEP 2 (row 2) and ERA-I (row 3). NCEP 1, which is generally drier than NCEP 2 shows a stronger upper layer (700–300 hPa) zonal moisture divergence with a peak in JJA, whereas the wettest reanalysis, ERA-I, displays the weakest. In the near-surface layer of the troposphere (1000–850 hPa), NCEP-1 and 2 depict peaks of moisture convergence in MAM and SON while ERA-I shows a stronger convergence of moisture throughout the year. For meridional component, all reanalyses consistently

produce a moisture convergence throughout the year with a maximum in JJA. The meridional moisture is stronger and more upward convergent than the zonal, justifying its prevalence in the contribution of total moisture flux. However, the shape of the total moisture is rather close to that of the zonal component. These results were also reported by Pokam et al. (2012). The opposite sign of upper and lower layer moisture fluxes is generally assigned to the presence in the region of Hadley and Walker type circulations (Pokam et al. 2012; Washington et al. 2013; Cook and Vizy 2016).

Even if basic climatology features (mode of seasonal and intra-seasonal variability) of model outputs of moisture fluxes are captured well, it is found that rainfall dry biases of CB are associated to an unrealistic simulated moisture amount. In fact, most RCM-runs (Fig S4) have simultaneously overestimated the zonal moisture divergence rate in the upper layer and underestimated the total column moisture convergence in the meridional component. The occurrence of the excessive moisture divergence fields in the upper layer is due to a higher outflow across western boundary (10°E) coupled to a weaker inflow through the eastern (35°E). Likewise, moisture advections across northern (10°N) and southern (10°S) frontiers are underestimated. However, processes controlling moisture amount are distinct across rainy seasons: In MAM, one of the wetter RCM-runs (RCA-EC-EARTH) shows the weakest western upper (lower) moisture divergence (convergence), but a strong eastern upper and lower inflow. The other, (RCA-NorESM1) features a high total moisture divergence column across western

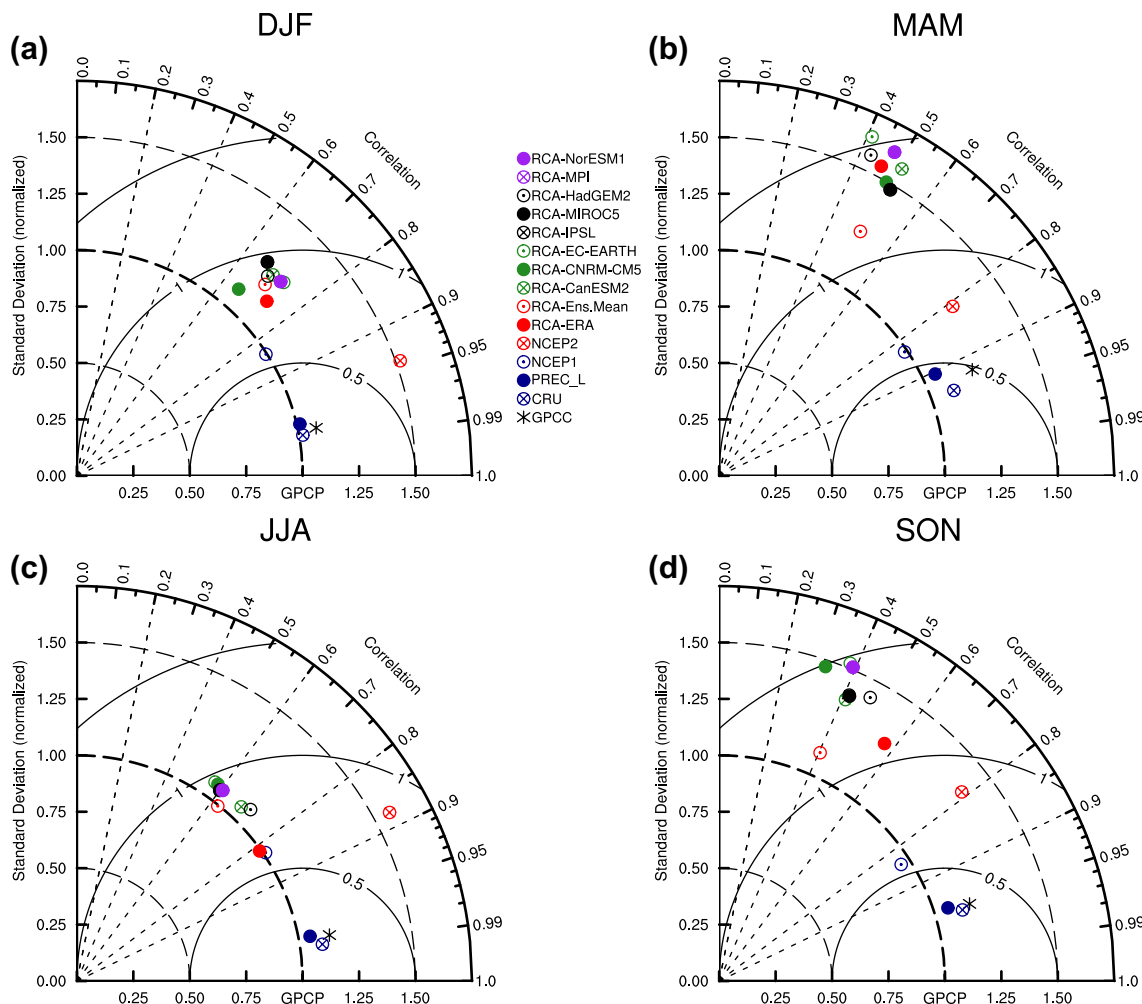


Fig. 4 Taylor diagrams displaying the statistics of monthly precipitation and comparing RCA4's experiments with observations GPCP (reference field), GPCC, CRU, PREC-L, NCEP-II, for the CB in **a** DJF, **b** MAM, **c** JJA and **d** SON seasons. The multi-model ensemble mean (RCA-Ens.Mean) and the evaluation simulation (RCA-ERA) are also shown for comparison

DJF, **b** MAM, **c** JJA and **d** SON seasons. The multi-model ensemble mean (RCA-Ens.Mean) and the evaluation simulation (RCA-ERA) are also shown for comparison

borderline, but compensated by a higher total moisture convergence column across eastern. Two configurations prevail in drier runs: some of them produce stronger western upper and lower outflows than eastern inflows (RCA-ERA, RCA-CanESM2, RCA-IPSL). The others (RCA-CNRM-CM5, RCA-MIROC5, RCA-HadGEM2 and RCA-MPI) present slight outflow through the western frontier, but rather a moderate inflow at east, which does not compensate for the exits from the west. In SON, all wetter RCM-runs (RCA-EC-EARTH, RCA-NorESM1, RCA-CNRM-CM5, RCA-MPI) depict higher inward moisture flux at east than outward at west. For drier experiments (RCA-ERA, RCA-HadGEM2, RCA-MIROC5, RCA-CanESM2, RCA-IPSL), the reverse situation occurs, but with some important distinctions. As instance, some drier simulations with moderate outflow (RCA-CanESM2, RCA-IPSL) extend upward the moisture divergence field. In DJF and JJA, the larger moisture divergence through west border is not met by the

eastern convergence moisture. At these times of year, all RCM-runs display an almost similar seasonality of transient flows across northern and southern boundaries. This suggest that the contribution of the meridional component to the CB rainfall biases is unimportant.

To highlight the strong influence of the upper zonal moisture divergence in the total rainfall amount, we have examined the mean-annual cycle of atmospheric moisture flux convergence, vertically integrated from 1000 to 300 hPa (Fig 6). As the ensemble mean of downscaled GCMs (RCA-EnsMean) is close to individual RCM-run, it has been chosen in place of all simulations, but the conclusion does not change. All data sets well depict the bimodal feature of total CB moisture fluxes convergence (Fig 6c), with maxima corresponding to both rainy seasons MAM and SON. Moreover, they are successful to proportionately link the wet character of each data set to the associated moisture convergence magnitude. However, the main discrepancy is confirmed

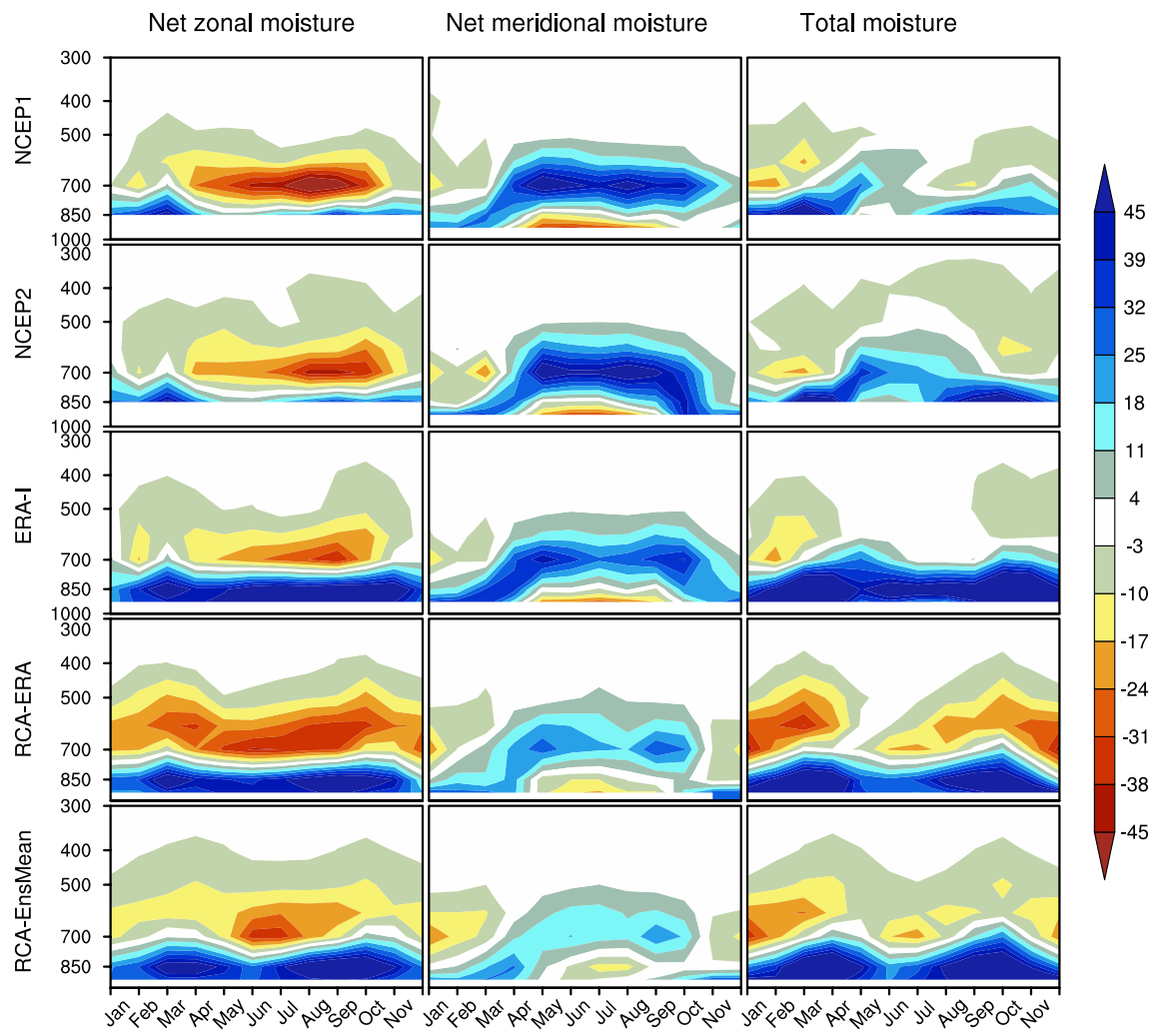


Fig. 5 Time–height sections of Net zonal (column 1), meridional (column 2) and total (column 3) moisture flux (in $10^{-8} \text{ kg m}^{-2} \text{ s}^{-1}$), summing the contribution of West–East [West (10°E) minus East

(35°E)] and South–North [South (10°S) minus North (10°N)] frontiers into CB. Negative values indicated moisture divergence and positive values convergence. See names of datasets left of panel

to be a weaker simulated moisture convergence rate due to the strong zonal divergence in the upper layer. In the zonal component, RCM-runs produce weaker moisture convergence peaks and stronger peaks of divergence (Fig 6a). In the meridional direction, the MAM peak is adequately captured, but the SON peak starts early and is slightly lower compared to NCEP2 and ERA-I (Fig 6b). Thus, CB rainfall dry biases are associated to a dry upper-tropospheric layer (Yin et al. 2013).

4.2 African easterly jets (AEJs)

We showed in the previous section that stronger modeled moisture fluxes divergence occur above 700 hPa, thus encompassing the field of interaction of the AEJs. The important role of the AEJ-N and AEJ-S in the supply of moisture flow into CB has already been established

(Nicholson and Grist 2003; Jackson et al. 2009; Pokam et al. 2012; Washington et al. 2013), and also shown in Fig 7 (rows 1–3). In this study, the signal of both jets is obtained by selecting over the domains $3\text{--}20^{\circ}\text{N}$ to $12\text{--}24^{\circ}\text{E}$ at 600–700 hPa for AEJ-N and $5\text{--}20^{\circ}\text{S}$ to $12\text{--}20^{\circ}\text{E}$ at 600 hPa for AEJ-S, all grid points where the u-wind speed $\geq 6 \text{ m s}^{-1}$ [shaded light blue color; following Nicholson and Grist (2003)]. The observed peak of moisture convergence in MAM is due to the presence of the northern component (AEJ-N) inside of the region, which supplies the domain through the northern boundary as a northeasterly flow. A semblable situation prevails in DJF, but with influx mostly from northeastern flank. However in JJA, the north influx declines owing to the position of AEJ-N out of the Basin, well depicted in ERA-I. At this time of year, the region is advected across the southeastern flank. Dyer et al. (2017) had identified this source of moisture from Indian Ocean as the most important

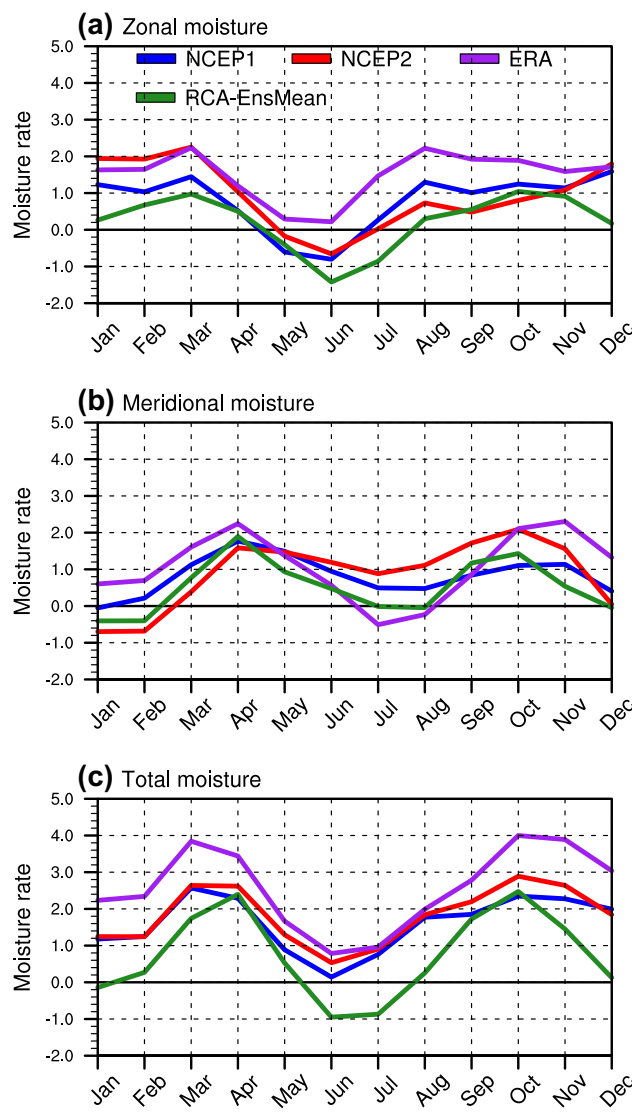


Fig. 6 The annual cycle of vertically integrated net water vapor flux (units: $10^{-5} \text{ kg m}^{-2} \text{s}^{-1}$), scaled by the area of the region: **a** zonal component (top), **b** meridional component (middle), and **c** total (bottom). Positive values indicate flux convergence and negative values flux divergence

for the CB. Jackson et al. (2009) showed that the southern component (AEJ-S) is the main driver of the intense convection over CB in SON, when the tropical easterly jet (TEJ) is strong and promotes much divergence flow around 200 hPa. Nicholson and Grist (2003) also shown that SON is the wettest season because of the existence of the two components of Jet at this period of year, that contribute to a more mid-level convergence into the region.

For this, and in order to explore drivers of the dry upper-tropospheric layer, we have assessed the influence of both AEJ branches on the upper layer moisture transport as sketched in Fig 7. Circulation patterns of moisture transport are similar between experiments (Fig S5) and the three

reanalysis products, but important differences exist in term of spatial extent and magnitude of jets. Almost all RCM-runs show an absence of both mid-tropospheric jets over the CB domain and place the beginning of AEJ-N area over the western frontier in all seasons. In fact, the northern branch appears above the west border, thus creating a strong divergent flow. At the same time at east, it is non-existent, which justifies a low rate of influx at this borderline. This is likewise illustrated by comparing the mean u-wind speed between the western and eastern limits as displayed in Fig. 8. One of RCM-runs that have featured the MAM maximum rainfall has not detected AEJs (RCA-EC-EARTH). The other has exhibited the best performance to model the AEJ-N component (RCA-NorESM1). Our interpretation is that, the atmospheric water budget is not unbalanced by excessive outflows through the western border (RCA-EC-EARTH) or else stronger western divergence moisture is mitigated by eastern convergence (RCA-NorESM1).

5 Projected changes under 1.5 °C and 2.0 °C GWLs

This section examines moisture convergence changes to understand drivers of projected rainfall changes, focusing on MAM and SON transition seasons, from the ensemble mean of all forcings (RCA-EnsMean), and from individual RCM runs (see panels in the supporting information). MAM and SON are the highest interest seasons for climate study over the CB because they are the two main rainy seasons of the region, and encompass the majority of processes that control local climate. Panels display changes at 1.5 °C (column 1) and 2 °C (column 2) GWLs, and the difference between the 1.5 °C and 2 °C warming levels (column 3).

5.1 Precipitation changes

Figure 9 shows projected changes in the mean seasonal MAM (rows 1) and SON (rows 2) rainfall under RCP4.5 (Fig. 9a) and RCP8.5 (Fig. 9b) warming scenarios. Projected changes differ as a function of region, of different RCM runs (see Supporting information), and of GWLs. RCM runs consensus is large for a moderated significant decrease in MAM rainfall at the two GWLs. Some exceptions of increased rainfall are projected over Gulf of Guinea and over the Ethiopian highlands. Two runs (RCA-MIROC5 and RCA-NorESM1-M, see Fig S6) also project an increase in rainfall in the southern part of the domain. The situation is different in SON where precipitation heterogeneously projected are larger than in MAM. Here, four runs (RCA-MIROC5, RCA-HadGEM2, RCA-MPI and RCA-NorESM1, see Fig S7) show that coastal regions are projected to moisten. Notably, there is an increase of

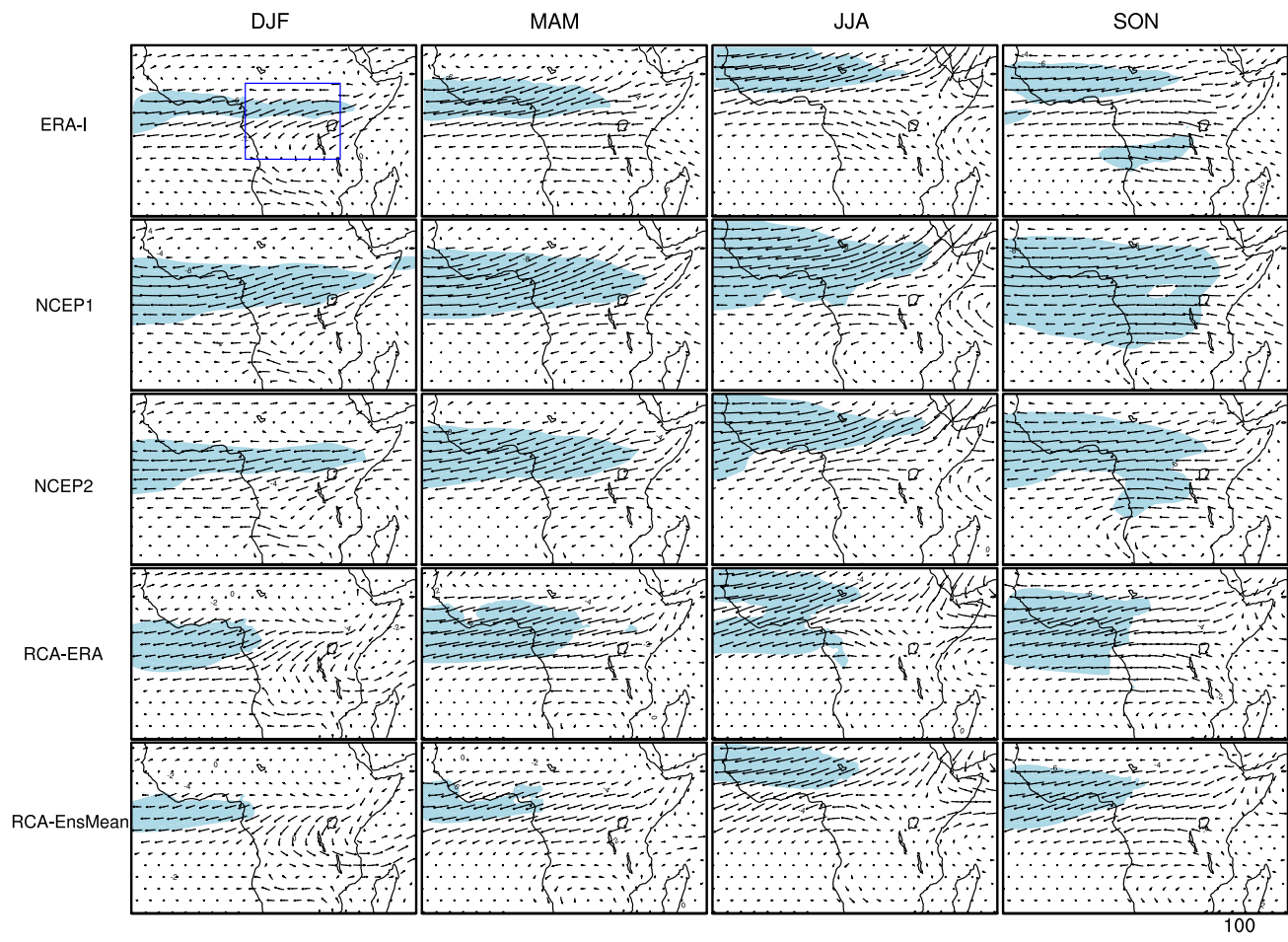


Fig. 7 Vertically integrated water vapor flux ($\text{kg m}^{-1} \cdot \text{s}^{-1}$) in the upper layer (850 to 300 hPa) in seasons DJF (column 1), MAM (column 2), JJA (column 3) and SON (column 4). Shaded light-blue area

(u-wind speeds $\geq 6 \text{ m s}^{-1}$) indicates the mean position of the jet. See names of datasets left of panel. The blue box denotes Congo Basin region

rainfall amount under RCP8.5 compared to RCP4.5, thus proving the rise of heavy rainfall under RCP8.5 warming scenario. Using the comparison 2 °C–1.5 °C warming level under RCP4.5, it's found that stronger rainfall increases (decreases) over northwestern (southern and eastern) flanks are expected at 2 °C GWL in MAM, but there are rather localised increases or decreases in SON. Little agreements are found amongst experiments: three runs (CanESM2, CNRM-CM5 and EC-EARTH) show that precipitation decrease over the northern part and coastal region is projected to moderate under 2 °C GWL; however, over CB and southern flank, the decrease is projected to strengthen according to all experiments. Under RCP8.5, the 2 °C GWL promotes a more decrease rainfall compared to 1.5 °C. These changes could suggest modifications in the origins and transport process of moisture flux. For more enlightenment, we have investigated changes in the contribution across different borderlines and in the spatial pattern of total moisture transport.

5.2 Moisture convergence changes

Contributions to the CB moisture through different frontiers in the zonal (rows 1) and meridional (rows 2) directions under RCP4.5 and RCP8.5 warming scenarios are shown respectively in Fig. 10a, b (also see Figures S8 and S9 for individual runs). These figures represent the annual variability in the column stratification of atmospheric moisture convergence (positive values) or divergence (negative values). Changes in the net zonal moisture show a strengthening in the upper layer moisture divergence. This implies an increase outflow (decrease inflow) through the west (east) boundary. However in the lower layer, RCM runs show limited consensus on the magnitude of slight increase moisture convergence, stronger in SON than MAM (see columns 2–3 in Figure S8). Concerning the net meridional moisture, most RCM runs are consistent on an increase in the MAM and SON upper and lower layers moisture convergence, stronger in MAM in the lower layer but in SON in the upper (see

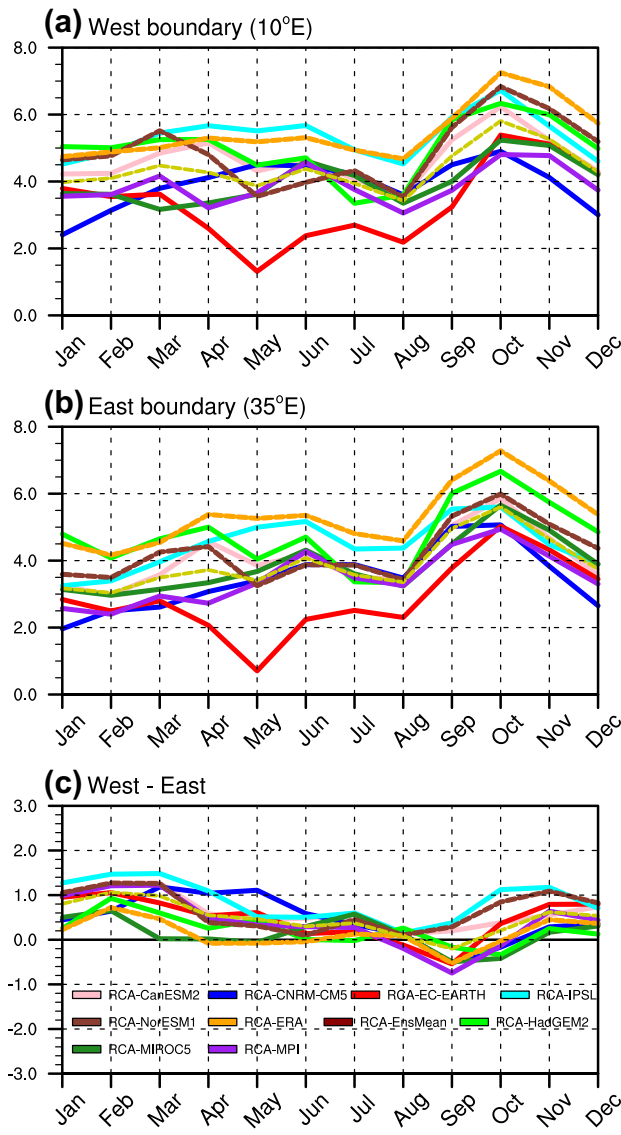


Fig. 8 Mean (600–700 hPa) u-wind speed at **a** West border and **b** East border. Also shown is the difference **c** West (10°E) minus East (35°E) to compared the u-wind speed at both boundaries

columns 2-3 in Figure S9). This is due to a strong increase inflow across northern boundary whereas no substantial change is found on the southern borderline. The most notable difference between the two GWLs is the stronger upper zonal moisture divergence under 2°C GWL, added to a strengthening of moisture convergence in the meridional direction (see column 4 in Fig. 10a, b). This is further discussed in the next paragraph.

To quantify the uncertainty rate associated to these projections, ranges of divergence values across runs are summarized in Fig. 11. Owing to the inconsistent atmospheric circulation pattern in the lower (1000–850 hPa) and upper (700–300 hPa) troposphere, the analysis was performed on these two layers, considering for each case the

two components. For the lower layer, its zonal component generally shows that all experiments tend to be robust from April to September, with the median value clearly distant from the reference line for both RCPs and GWLs. Here, the moisture convergence increases throughout the year with peak observed during JJA and more pronounced at 2°C . On the other hand, its meridional component consistently project a robust change all the year according to both RCPs and GWLs. Although during the JJA season, the zonal and meridional components have changes of opposite sign, the divergence of the meridional flow is more important than the convergence of the zonal flow. Concerning the upper layer, its zonal component shows that the moisture divergence will consistently increase throughout the year for all RCM runs. On the contrary, its meridional component generally shows little or no change, except from June to October when a slight increase in moisture convergence is noted. The comparative analysis of the mean change between 1.5°C and 2°C GWLs reveals different responses in the two RCPs. In RCP4.5, changes are more prominent for 2°C relative to 1.5°C with highest moisture convergence (divergence) found in lower (upper) layer. In RCP8.5, there is not a clear consensus between the two GWLs throughout the year, except in October when a strongest increase in zonal moisture convergence is predicted. This can suggest the intensification of extreme precipitation events under RCP8.5 (Fotso-Nguemo et al. 2018).

To further understand mechanisms of change associated to the atmospheric circulation in the both layers, we have examined mean changes in moisture transport respectively at 925 hPa (Fig. 12) and at 700 hPa (Fig. 13); (also see Figures S10–S14 for individual RCM-runs responses). It's found that these two individual levels strongly contribute to the moisture advection into the region (Pokam et al. 2012; Creese and Washington 2016; Dyer et al. 2017) added to the important role of the divergent circulation at 850 hPa in the low level westerly (LLW) flow from Atlantic Ocean into the continent (Pokam et al. 2014; James et al. 2018). Figure 12a shows that in the lower level under RCP4.5, the intensification of advected moisture from Atlantic Ocean toward the continent for the two seasons is stronger than the slight increase easterly flow and more pronounced for 2.0°C GWL. However under RCP8.5 (Fig. 12b), while the LLW flow decreases for 1.5°C , there is rather an increase inflow for 2°C GWL. A similar response also occurs in the easterly flow. In the upper layer (Fig. 13), the MAM and SON easterly divergent transports are projected to strengthen according to all RCPs. The comparative analysis 2°C vs 1.5°C reveals a heaviest divergent flow under 2.0°C GWL.

There appears to be evidence that the projected dry and wet conditions in RCA4 experiments over CB are consistent with changing processes of moisture transport during both rainy seasons. Furthermore, these processes agree with

Fig. 9 Projected changes in mean seasonal MAM (rows 1) and SON (rows 2) rainfall (in mm/day) under **a** RCP4.5 and **b** RCP8.5 warming scenarios. Columns 1 and 2 are respectively changes at 1.5 °C and 2 °C GLWs with respect to CTL, while the difference between the changes at 2 °C and 1.5 °C GWLs is shown in column 3. Stippling indicates 95% significance level using t-test. The black box denotes CB region

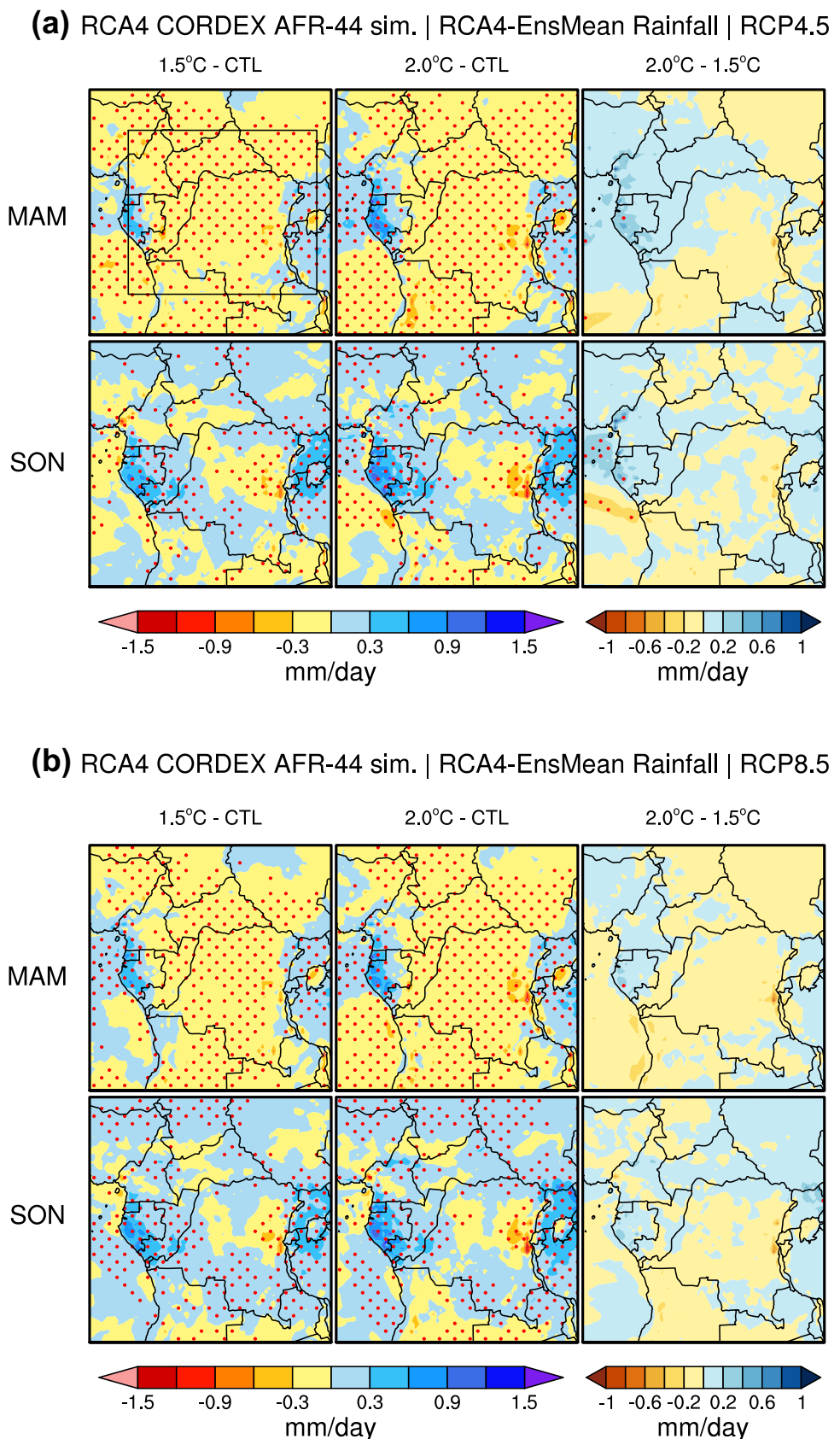
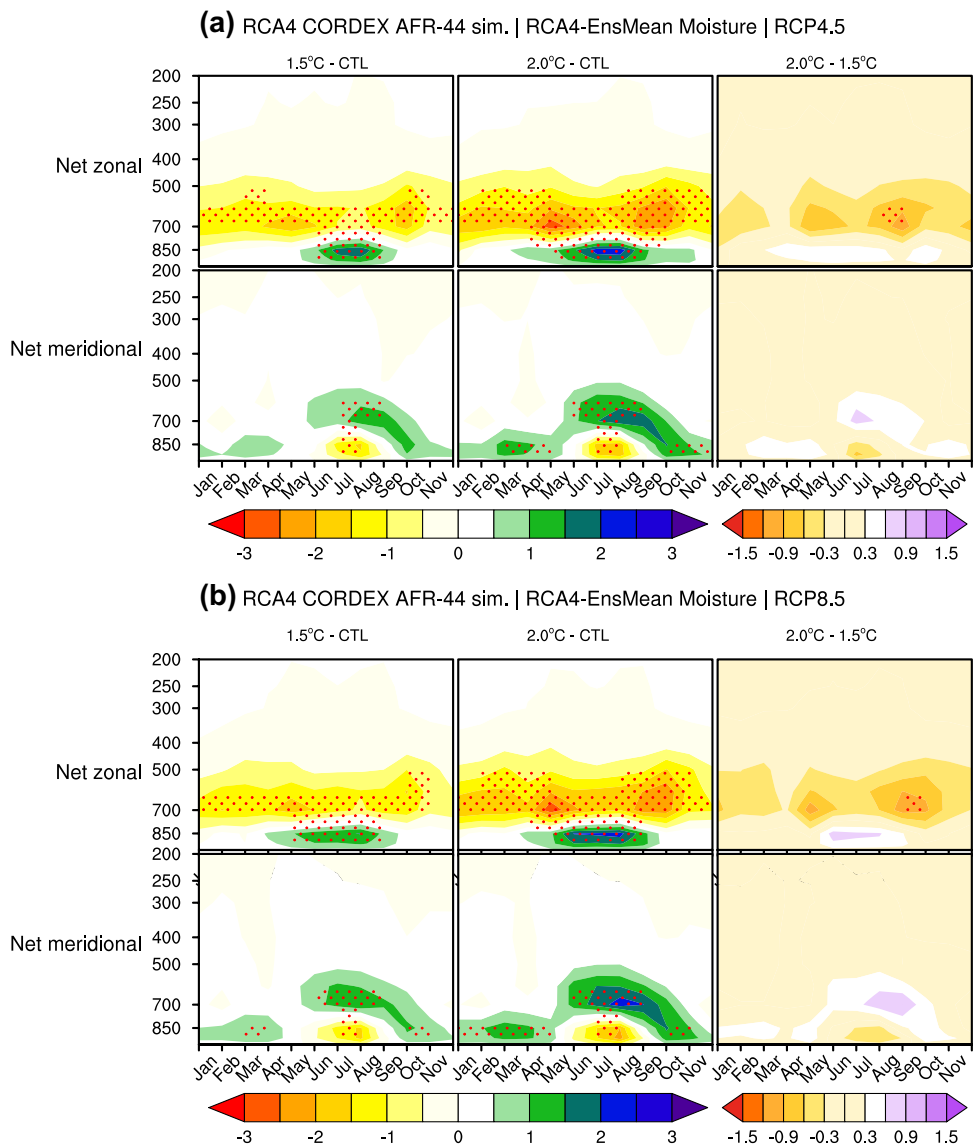


Fig. 10 Time-height sections of net zonal (rows 1) and net meridional (rows 2) moisture flux (in $10^{-8} \text{ kg m}^{-2} \text{ s}^{-1}$), summing respectively the contributions of West-East (West (10°E) minus East (35°E)) and South-North (South (10°S) minus North (10°N)) frontiers into CA, scaled by the surface area of the region under **a**) RCP4.5 and **b**) RCP8.5 warming scenarios. Negative values indicated moisture divergence and positive values convergence. Stippling indicates 95% significance level using t-test



drivers of wet and dry conditions as demonstrated in Washington et al. (2013). The drier season MAM is connected to a great increase in zonal moisture divergence in the upper layer, which is stronger than the upper and lower convergence in the meridional component. In the wettest season SON, the strong upper zonal divergence is moderated by a strong upper and lower zonal/meridional convergence.

6 Discussion and conclusions

A comprehensive assessment of RCA4 responses to eight CMIP5 forcing fields over the Congo Basin is presented in this study. Sources of modeled rainfall biases were studied, as well as drivers of expected rainfall changes under global warming of 1.5°C and 2°C .

Under the historical climate, there are variation between models in simulated climatology, larger for driving GCMs than corresponding RCM-runs, and more pronounced in rainy seasons. Although RCA4 models dry biases over the CB, it well captures observed features of the real climate, including seasonal and intra-seasonal variability of rainfall patterns, more consistent in dry seasons. Furthermore, comparing the climatology feature for individual experiments to those of the “evaluation” experiment and RCM ensemble model, similar features emerge, thus confirming the hypothesis of systematic biases as main sources for model’s errors. Recently, Creese and Washington (2016) argued that the ensemble model from CMIP5 is not appropriated to model Congo rainfall due to the divergences of climatology features across models. Our findings show that the downscaling using a common RCM is a plausible option to overcome to this

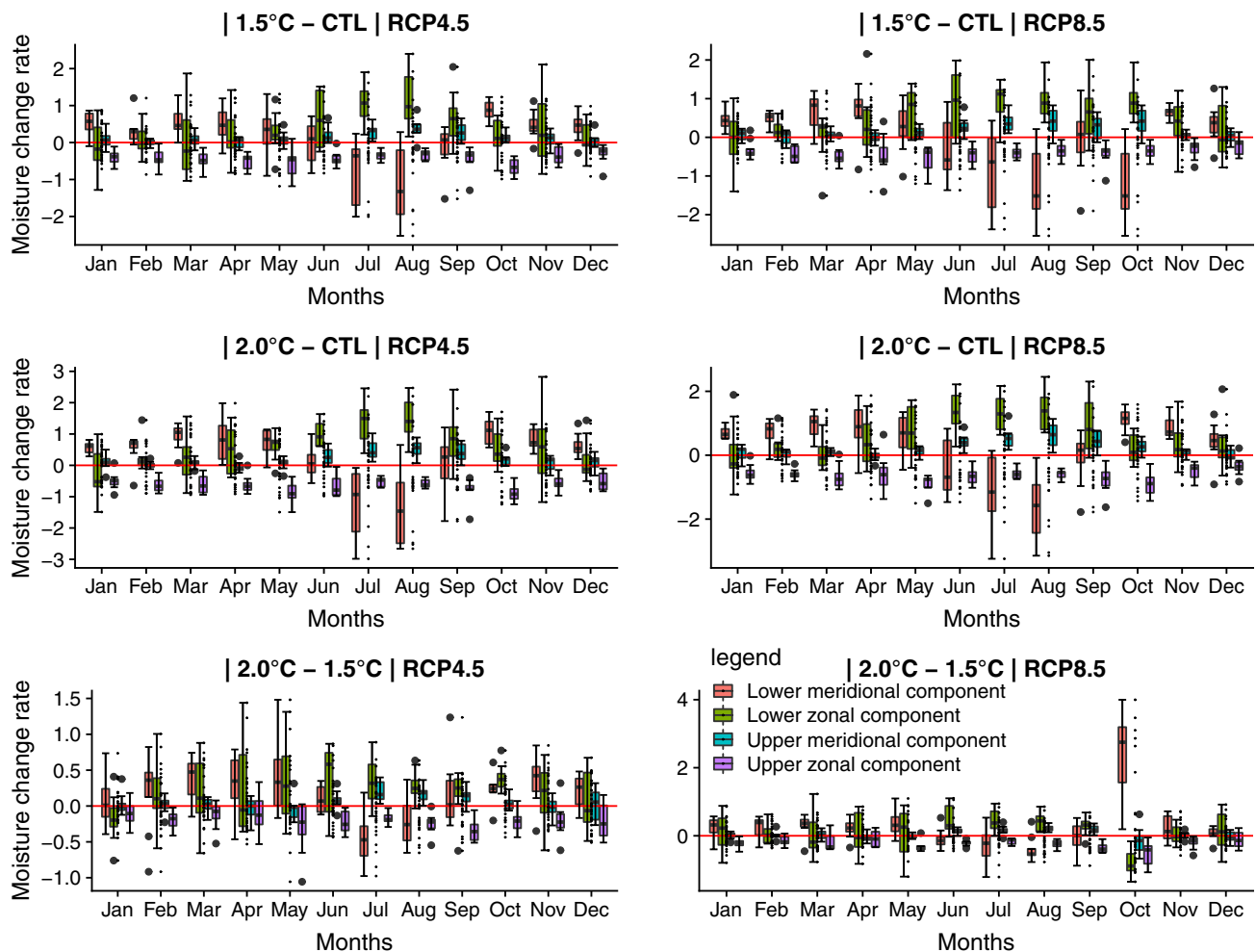


Fig. 11 Uncertainty ranges in projected changes in the zonal and meridional moisture in the bottom (975–850 hPa) and upper (700–300 hPa) layers at 1.5 °C and 2.0 °C GWLs under RCP4.5 (column

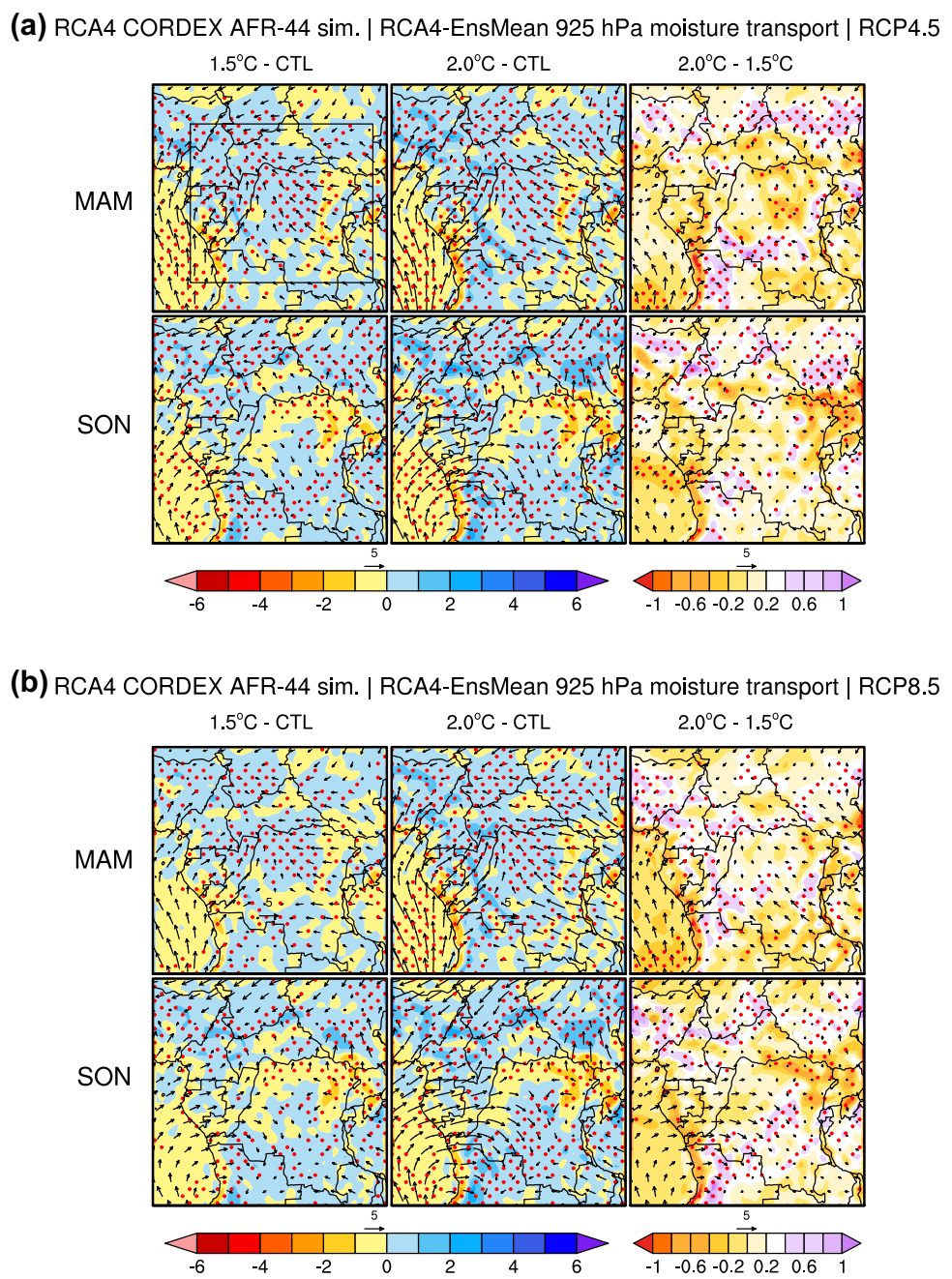
1) and RCP8.5 (column 2). Comparative analysis 2.0 °C vs 1.5 °C is also shown. Negative values indicated moisture divergence and positive values convergence

issue, in the case the RCM exhibits a good skill to reproduce the real climate.

By using the process-based assessment method with a special focus on the climatology feature of moisture convergence, we have established that CB rainfall dry biases are associated with an excessive moisture divergence in the upper layer troposphere, driven by mid-tropospheric jets. Indeed AEJs suddenly appeared at the western boundary (stronger outflows), but is strongly underestimated at the eastern frontier (weaker inflows), which unbalances the water balance equation. This reinforces previous findings of Nicholson (2009) who showed that during the dry year, AEJ-N is located more westward and is weaker compared to the wet year. Recently Hua et al. (2019) by assessing reanalysis products over Central Equatorial Africa, have also shown that differences in the lower and mid-tropospheric moisture transport are prospective causes of differences in the observed rainfall amount. AEJ-N decreases (increases)

the upper layer zonal (meridional) moisture divergence (convergence) when it crosses the northern part of CB region (Pokam et al. 2012). Over Amazonia, Yin et al. (2013) evenly found that CMIP5 models of moisture convergence and surface evapotranspiration are positively correlate with total rainfall. This suggests the need for additional studies on the other sources of CB moisture and other parameters that modulate the rainfall. For example, Although they have reported different results, some work has identified local evaporation sources as the main component of rainfall over that region, as it is in major part forested e.g. (Trenberth 1999; Van der Ent et al. 2010; Pokam et al. 2012; Dyer et al. 2017). Likewise, the influences of Atlantic and Indian Ocean sea surface temperatures (SSTs) in the CB rainfall variability is no longer in doubt. Creese and Washington (2018) showed that Atlantic SST biases is one of most important causes of differences between wet and dry models in the western part, but do not the case at east. On the East sector, they found

Fig. 12 Mean seasonal MAM (rows 1) and SON (rows 2) of total moisture transport at 925 hPa (vector in $\text{kg m}^{-1} \text{s}^{-1}$) and total moisture flux divergence (shaded contours in $10^{-8} \text{ kg m}^{-2} \text{s}^{-1}$) under **a** RCP4.5 and **b** RCP8.5. Stippling indicates 95% significance level using t-test. The black box denotes CB region



that the dynamical circulation of the region like the low-level westerly flow, which constitutes the lower branch of an Atlantic-Congo overturning circulation plays a dominant role in determining region wetness or dryness.

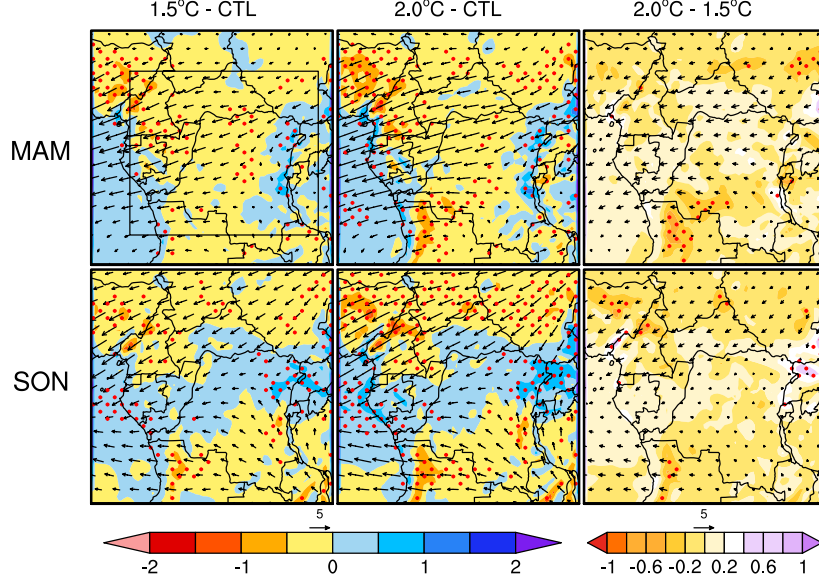
Under the future climate, results show that RCA4 simulates a moderated decrease in MAM rainfall inland of CB. In SON, projected precipitation are expected to locally decrease or increase, and larger than MAM. These changes are found to associate with modifications in the dynamic of moisture transport in the upper and lower layers troposphere. Most runs agree that the decrease of MAM rainfall is associated with an increase in the upper layer divergence

zonal moisture, stronger than an increase in the meridional moisture convergence at this time of year. In SON, an opposite tendency is projected, added to the localised decreases/increases moisture divergence/convergence. Future CB moisture seems to be more affected in the zonal component. Furthermore, the projected zonal moisture divergence tend to be stronger under 2 °C GWL than 1.5 °C, more pronounced under RCP8.5 warming scenario and means an increased in risk associated with 2 °C.

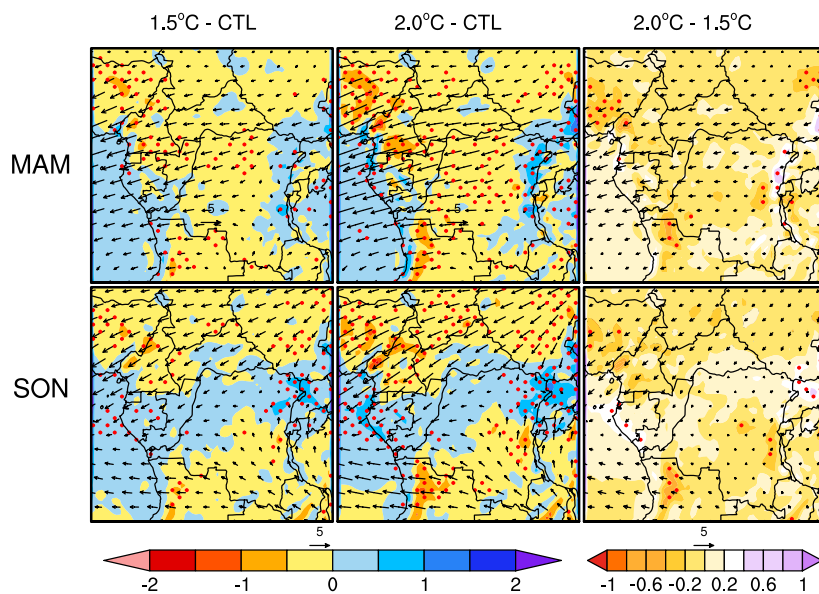
Previous work has investigated the effects of global warming using various climate models and climate parameters over Central Africa. Using ten RCMs, Weber et al.

Fig. 13 Same as Fig. 12, but at 700 hPa

(a) RCA4 CORDEX AFR-44 sim. | RCA4-EnsMean 700 hPa moisture transport | RCP4.5



(b) RCA4 CORDEX AFR-44 sim. | RCA4-EnsMean 700 hPa moisture transport | RCP8.5



(2018) found an increase projected daily rainfall intensity toward higher global warming scenarios between 15°S–15°N latitudes, especially for Sub-Saharan coastal regions. Considering a subset of CMIP5 GCMs, Diedhiou et al. (2018) shown that CA will face a small change in total rainfall, but the length of wet spells is projected to decrease, added to a strong increase of extreme rainfall. This is consistent with findings of Tamoffo et al. (2019) who reported significant decrease in the frequency of wet days. While Fotso-Nguemo et al. (2016) found a projected decrease rainfall over most inlands using REMO model, Aloysius et al. (2016) contrariwise reported an increase in precipitation using an ensemble

mean of CMIP5 models. Pokam et al. (2018) also found a projected decrease in rainfall over much of inland during MAM. Others climate models (e.g. CCLM see Dosio and Panitz (2016) have depicted consistent signal of climate change in rainfall trend across different forcings, but an opposite sign relative to corresponding driving GCMs. Results presented in this study agree with those showing projected drier conditions in MAM relative to SON, but driven by upstream changes in moisture dynamics.

Thus, regional responses to global warming differ across models and there are large uncertainties associated to projections over Central Africa. The robustness and responses to

global warming differ as a function of the considered variable and of the RCM–GCM combination. However, despite uncertainties in mean precipitation, most studies referenced above have shown a projected increase in extreme events. By looking in precipitation changes, experiment projections are less sensitive when moving from 1.5 °C to 2 °C GWLs. However, an obvious intensification of moisture divergence (convergence) in the zonal (meridional) component is observed at 2 °C relative to 1.5 °C. This can imply serious repercussions in extreme rainfall events and might cause disastrous consequences on future water resource management, agriculture and food security. This highlights the benefits of limiting warming at 1.5 °C rather than 2 °C in order to reduce the risks of disasters associated to global warming.

Here we show that the strengthening of moisture divergence is strongly contributed in the upper zonal direction and could be related to a change in mid-tropospheric jet circulation (Nicholson and Grist 2003). Furthermore, the important role of the Walker and Hadley type overturning circulations in processes generating rainfall over the Congo Basin (e.g. Cook and Vizy 2016) and over Sahara e.g. (Grist and Nicholson 2001; Nicholson 2009; Neupane 2016) regions has been already highlighted in previous studies. Notably over the Maritime Continent and central equatorial Pacific, Tokinaga et al. (2012) showed that the significant decrease in land precipitation and marine cloudiness are due to a weakening of Walker circulation. This draw attention to how CB Walker and Hadley type circulations will respond to global warming at 1.5 °C and 2 °C GWLs. In addition, a recent study by Sun and Wang (2018a, b) has revealed an enhanced connection between regional and global climate system under global warming. These questions should be also addressed over CB to increase our knowledge on how changes in atmospheric circulation will affect future climate under the global warming. These will be addressed in future work.

Based on the climatology study, the model features peak rainfall in the west, but this is not necessarily the case for observations (Fig. 2) and other models, some of which have peaks in the east (Creese and Washington 2018). There are uncertainties in the pattern and magnitude of future change, other models likely show larger changes in east. Notably, it's important to precise that our findings are just indicative for this particular model, and do not explore full range of uncertainties in future projections over CB. Moreover, Nikulin et al. (2018) also argued on the subjectivity of the selection control period which may conducts to dissimilar deductions on future climate effects at the identical GWLs. Additional studies using other climate models are needed to establish the robustness of these investigations. These results must be also interpreted taking into account the agreement level between RCM runs and observed datasets under the current climate. Nevertheless, although only one RCM is used, there

is some divergence between RCM's forcings with different GCMs. This is useful to explore some uncertainties as those linked to boundary conditions or RCM's internal processes. Furthermore, this work also demonstrates (1) the importance of understanding how models behave before analysing their future projections; (2) shows a methodology for doing so, and processes to analyse over CB and (3) helps to understand the bias in this specific model—which could inform model development.

Acknowledgements The constructive comments and suggestions of the editor and two anonymous reviewers led to several key improvements of the first version of the manuscript. The first author wish to express their gratitude to very fruitful discussions with F. Guichard (CNRM). The authors would like to acknowledge support from the Swedish Government through the Swedish International Development Cooperation Agency (SIDA). This work is partially supported by the International Joint Laboratory's research "Dynamics of Land Ecosystems in Central Africa: A Context of Global Changes" (IJL DYCOCA/LMI DYCOFAC). GNL acknowledges support by PREFACE project (EU FP7/2007-2013 under grant agreement no. 603521); National Research Foundation SARCHI Chair in Ocean-Atmosphere-Land modelling and ACCESS project. We also acknowledge logistical support from the CORDEX International Project Office, the Swedish Meteorological Institute and the Climate System Analysis Group at the University of Cape Town. We are grateful to all the modeling groups that performed the simulations and made their data available.

References

- Aloysius NR, Sheffield J, Saiers JE, Li H, Wood EF (2016) Evaluation of historical and future simulations of precipitation and temperature in central Africa from CMIP5 climate models. *J Geophys Res Atmos* 121(1):130–152. <https://doi.org/10.1002/2015JD023656>
- Baccini A, Goetz SJ, Walker WS, Laporte NT, Sun M, Sulla-Menashe D, Hackler J, Beck PSA, Dubayah R, Friedl MA, Samanta S, Houghton RA (2012) Estimated carbon dioxide emissions from tropical deforestation improved by carbon-density maps. *Nat Clim Change*. <https://doi.org/10.1038/nclimate1354>
- Baumberger C, Knutti R, Hirsch Hadorn G (2017) Building confidence in climate model projections: an analysis of inferences from fit. *Wiley Interdiscip Rev Clim Change* 8(3):e454. <https://doi.org/10.1002/wcc.454>. <https://onlinelibrary.wiley.com/doi/abs/10.1002/wcc.454>
- Bentsen M, Bethke I, Debernard J, Iversen T, Kirkevåg A, Seland Ø, Drange H, Roelandt C, Seierstad I, Hoose C et al (2013) The Norwegian earth system model, NORESM1—part 1: description and basic evaluation of the physical climate. *Geosci Model Dev* 6(3):687–720. <https://doi.org/10.5194/gmd-6-687-2013>
- Birch CE, Parker D, Marsham J, Copsey D, Garcia-Carreras L (2014) A seamless assessment of the role of convection in the water cycle of the West African monsoon. *J Geophys Res Atmos* 119(6):2890–2912. <https://doi.org/10.1002/2013JD020887>
- Chylek P, Li J, Dubey M, Wang M, Lesins G (2011) Observed and model simulated 20th century arctic temperature variability: Canadian earth system model CanESM2. *Atmos Chem Phys Discuss* 11(8):22,893–22,907. <https://doi.org/10.5194/acpd-11-22893-2011>
- Collins WJ, Bellouin N, Doutriaux-Boucher M, Gedney N, Halloran P, Hinton T, Hughes J, Jones CD, Joshi M, Liddicoat S, Martin

- G, O'Connor F, Rae J, Senior C, Sitch S, Totterdell I, Wiltshire A, Woodward S (2011) Development and evaluation of an earth-system model HadGEM2. *Geosci Model Dev* 4(4):1051–1075. <https://doi.org/10.5194/gmd-4-1051-2011>. <https://www.geosci-model-dev.net/4/1051/2011/>
- Cook KH (1999) Generation of the African easterly jet and its role in determining west African precipitation. *J Clim* 2(5):1165–1184. <https://doi.org/10.1175/1520-0442>. [https://doi.org/10.1175/1520-0442\(1999\)012<1165:GOTAEJ>2.0.CO;2](https://doi.org/10.1175/1520-0442(1999)012<1165:GOTAEJ>2.0.CO;2)
- Cook KH, Vizy EK (2016) The Congo Basin Walker circulation: dynamics and connections to precipitation. *Clim Dyn* 47(3):697–717. <https://doi.org/10.1007/s00382-015-2864-y>
- Creese A, Washington R (2016) Using qflux to constrain modeled congo basin rainfall in the CMIP5 ensemble. *J Geophys Res Atmos* 121(22):13,415–13,442. <https://doi.org/10.1002/2016JD025596>
- Creese A, Washington R (2018) A process-based assessment of CMIP5 rainfall in the Congo Basin: the September–November rainy season. *J Clim* 31(18):7417–7439. <https://doi.org/10.1175/JCLI-D-17-0818.1>
- Crétat J, Vizy EK, Cook KH (2014) How well are daily intense rainfall events captured by current climate models over Africa? *Clim Dyn* 42(9):2691–2711. <https://doi.org/10.1007/s00382-013-1796-7>
- Dargie GC, Lewis SL, Lawson IT, Mitchard ET, Page SE, Bocko YE, Ifo SA (2017) Age, extent and carbon storage of the central Congo Basin peatland complex. *Nature* 542(7639):86. <https://doi.org/10.1038/nature21048>
- Dee DP, Uppala SM, Simmons AJ, Berrisford P, Poli P, Kobayashi S, Andrae U, Balmaseda MA, Balsamo G, Bauer P, Bechtold P, Beljaars ACM, van de Berg L, Bidlot J, Bormann N, Delsol C, Dragani R, Fuentes M, Geer AJ, Haimberger L, Healy SB, Hersbach H, HV, Isaksen L, Kberg P, Khler M, Matricardi M, McNally AP, Monge-Sanz BM, Morcrette JJ, Park BK, Peubey C, de Rosnay P, Tavolato C, Thépaut JN, Vitart F (2011) The era-interim reanalysis: configuration and performance of the data assimilation system. *Q J R Meteorol Soc* 137(656):553–597. <https://doi.org/10.1002/qj.828>. <https://rmts.onlinelibrary.wiley.com/doi/abs/10.1002/qj.828>
- Dezfouli AK, Nicholson SE (2013) The relationship of rainfall variability in western equatorial Africa to the tropical oceans and atmospheric circulation. Part II: the boreal autumn. *J Clim* 26(1):66–84. <https://doi.org/10.1175/JCLI-D-11-00686.1>
- Dezfouli AK, Zaitchik BF, Gnanadesikan A (2015) Regional atmospheric circulation and rainfall variability in south equatorial Africa. *J Clim* 28(2):809–818. <https://doi.org/10.1175/JCLI-D-14-00333.1>
- Diaconescu EP, Laprise R (2013) Can added value be expected in RCM-simulated large scales? *Clim Dyn* 41(7):1769–1800. <https://doi.org/10.1007/s00382-012-1649-9>
- Diallo I, Sylla M, Giorgi F, Gaye A, Camara M (2012) Multimodel GCM-RCM ensemble-based projections of temperature and precipitation over west Africa for the early 21st century. *Int J Geophys* 2012:1–19. <https://doi.org/10.1155/2012/972896>. <http://downloads.hindawi.com/journals/ijgp/2012/972896.pdf>
- Diallo I, Giorgi F, Deme A, Tall M, Mariotti L, Gaye AT (2016) Projected changes of summer monsoon extremes and hydroclimatic regimes over west Africa for the twenty-first century. *Clim Dyn* 47(12):3931–3954. <https://doi.org/10.1007/s00382-016-3052-4>
- Diedhiou A, Bichet A, Wartenburger R, Seneviratne SI, Rowell DP, Sylla MB, Diallo I, Todzo S, Touré NE, Camara M, Ngatchah BN, Kane NA, Tall L, Affholder F (2018) Changes in climate extremes over west and central Africa at 1.5 °C and 2 °C global warming. *Environ Res Lett* 13(6):065020. <http://stacks.iop.org/1748-9326/13/i=6/a=065020>
- Dosio A, Panitz HJ (2016) Climate change projections for CORDEX-Africa with COSMO-CLM regional climate model and differences with the driving global climate models. *Clim Dyn* 46(5):1599–1625. <https://doi.org/10.1007/s00382-015-2664-4>
- Dufresne JL, Foujols MA, Denvil S, Caubel A, Marti O, Aumont O, Balkanski Y, Bekki S, Bellenger H, Benshila R, Bony S, Bopp L, Braconnot P, Brockmann P, Cadule P, Cheruy F, Codron F, Cozic A, Cugnet D, de Noblet N, Duvel JP, Ethé C, Fairhead L, Fichefet T, Flavoni S, Friedlingstein P, Grandpeix JY, Guez L, Guilyardi E, Hauglustaine D, Hourdin F, Idelkadi A, Ghattas J, Joussaume S, Kageyama M, Krinner G, Labetoulle S, Lahellec A, Lefebvre MP, Lefevre F, Levy C, Li ZX, Lloyd J, Lott F, Madec G, Mancip M, Marchand M, Masson S, Meurdesoif Y, Mignot J, Musat I, Parouty S, Polcher J, Rio C, Schulz M, Swingedouw D, Szopa S, Talandier C, Terray P, Viovy N, Vuichard N (2013) Climate change projections using the IPSL-CM5 earth system model: from CMIP3 to CMIP5. *Clim Dyn* 40(9):2123–2165. <https://doi.org/10.1007/s00382-012-1636-1>
- Dyer EL, Jones D, Nusbaumer J, Li H, Collins O, Vettoretti G, Noone D (2017) Congo Basin precipitation: assessing seasonality, regional interactions, and sources of moisture. *J Geophys Res Atmos*. <https://doi.org/10.5194/esd-2017-91>
- Fisher JB, Sikka M, Sitch S, Ciais P, Poultre B, Galbraith D, Lee JE, Huntingford C, Viovy N, Zeng N, Ahlström A, Lomas MR, Levy PE, Frankenberg C, Saatchi S, Malhi Y (2013) African tropical rainforest net carbon dioxide fluxes in the twentieth century. *Philos Trans R Soc B Biol Sci*. <https://doi.org/10.1098/rstb.2012.0376>. <http://rstb.royalsocietypublishing.org/content/368/1625/20120376>
- Flato G, Marotzke J, Abiodun B, Braconnot P, Chou SC, Collins WJ, Cox P, Driouech F, Emori S, Eyring V, Forest C, Gleckler P, Guilyardi E, Jakob C, Kattsov V, Reason C, Rummukainen M (2013) Evaluation of climate models. In: Climate change 2013: the physical science basis. contribution of working group I to the fifth assessment report of the intergovernmental panel on climate change. Assessment reports of IPCC, vol 5. Cambridge University Press, pp 741–866. <http://elib.dlr.de/95697/>
- Fotso-Nguemo TC, Vondou DA, Tchawoua C, Haensler A (2016) Assessment of simulated rainfall and temperature from the regional climate model remo and future changes over central Africa. *Clim Dyn* 48(11):3685–3705. <https://doi.org/10.1007/s00382-016-3294-1>
- Fotso-Nguemo TC, Vondou DA, Pokam WM, Djomou ZY, Diallo I, Haensler A, Tchotchou LAD, Kamsu-Tamo PH, Gaye AT, Tchawoua C (2017) On the added value of the regional climate model REMO in the assessment of climate change signal over central Africa. *Clim Dyn* 49(11):3813–3838. <https://doi.org/10.1007/s00382-017-3547-7>
- Fotso-Nguemo TC, Chamani R, Yepdo ZD, Sonkoué D, Matsaguim CN, Vondou DA, Tanessong RS (2018) Projected trends of extreme rainfall events from CMIP5 models over central Africa. *Atmo Sci Lett* 19(2):1–8. <https://doi.org/10.1002/asl.803>
- Gbobaniyi E, Sarr A, Sylla MB, Diallo I, Lennard C, Dosio A, Dhiédiou A, Kamga A, Klutse NAB, Hewitson B et al (2014) Climatology, annual cycle and interannual variability of precipitation and temperature in CORDEX simulations over west Africa. *Int J Climatol* 34(7):2241–2257. <https://doi.org/10.1002/joc.3834>
- Giannini A, Biasutti M, Held IM, Sobel AH (2008) A global perspective on African climate. *Clim Change* 90(4):359–383. <https://doi.org/10.1007/s10584-008-9396-y>
- Gibba P, Sylla MB, Okogbue EC, Gaye AT, Nikiema M, Kebe I (2018) State-of-the-art climate modeling of extreme precipitation over Africa: analysis of CORDEX added-value over CMIP5. *Theor Appl Climatol*. <https://doi.org/10.1007/s00704-018-2650-y>
- Giorgi F, Gutowski WJ (2015) Regional dynamical downscaling and the CORDEX initiative. *Annu Rev Environ Resour*

- 40(1):467–490. <https://doi.org/10.1146/annurev-environ-102014-021217>
- Giorgi F, Jones C, Asrar GR, et al (2009) Addressing climate information needs at the regional level: the CORDEX framework. *World Meteorol Org (WMO) Bull* 58(3):175. <http://wcrp.ipsl.jussieu.fr/cordex/documents/CORDEXgiorgiWMO.pdf>
- Giorgi F, Coppola E, Raffaele F, Diro GT, Fuentes-Franco R, Giuliani G, Mamgain A, Llopard MP, Mariotti L, Torma C (2014) Changes in extremes and hydroclimatic regimes in the CREMA ensemble projections. *Clim Change* 125(1):39–51. <https://doi.org/10.1007/s10584-014-1117-0>
- Gleckler PJ, Taylor KE, Doutriaux C (2008) Performance metrics for climate models. *J Geophys Res Atmos*. <https://doi.org/10.1029/2007JD008972>. <https://agupubs.onlinelibrary.wiley.com/doi/abs/10.1029/2007JD008972>
- Grist JP, Nicholson SE (2001) A study of the dynamic factors influencing the rainfall variability in the west African Sahel. *J Clim* 14(7):1337–1359
- Haensler A, Saeed F, Jacob D (2013) Assessing the robustness of projected precipitation changes over central Africa on the basis of a multitude of global and regional climate projections. *Clim Change* 121(2):349–363. <https://doi.org/10.1007/s10584-013-0863-8>
- Harris I, Jones P, Osborn T, Lister D (2014) Updated high-resolution grids of monthly climatic observations—the CRU TS3.10 dataset. *Int J Climatol* 34(3):623–642. <https://doi.org/10.1002/joc.3711>
- Hazeleger W, Severijns C, Semmler T, Stefanescu S, Yang S, Wang X, Wyser K, Dutra E, Baldasano JM, Bintanja R, et al (2010) EC-earth. *Bull Am Meteorol Soc* 91(10):1357–1364. <https://doi.org/10.1175/2010BAMS2877.1>
- Howard E, Washington R (2018) Characterising the synoptic expression of the Angola low. *J Clim*. <https://doi.org/10.1175/JCLI-D-18-0017.1>
- Hua W, Zhou L, Nicholson SE, Chen H, Qin M (2019) Assessing reanalysis data for understanding rainfall climatology and variability over central equatorial Africa. *Clim Dyn*. <https://doi.org/10.1007/s00382-018-04604-0>
- Huffman GJ, Adler RF, Bolvin DT, Gu G (2009) Improving the global precipitation record: GPCC version 2.1. *Geophys Res Lett*. <https://doi.org/10.1029/2009GL040000>. <https://agupubs.onlinelibrary.wiley.com/doi/abs/10.1029/2009GL040000>
- IPCC (2007) The physical science basis. summary for policymakers. contribution of working group I to the fourth assessment report of the intergovernmental panel on climate change. Jelektronnyj resurs. <http://www.ipcc.ch>
- Jackson B, Nicholson SE, Klotter D (2009) Mesoscale convective systems over western equatorial Africa and their relationship to large-scale circulation. *Mon Weather Rev* 137(4):1272–1294. <https://doi.org/10.1175/2008MWR2525.1>
- James R, Washington R, Rowell DP (2013) Implications of global warming for the climate of African rainforests. *Philos Trans R Soc B* 368(1625):20120,298. <https://doi.org/10.1098/rstb.2012.0298>
- James R, Washington R, Jones R (2015) Process-based assessment of an ensemble of climate projections for west Africa. *Jo Geophys Res Atmos* 120(4):1221–1238. <https://doi.org/10.1002/2014JD022513>. <https://agupubs.onlinelibrary.wiley.com/doi/abs/10.1002/2014JD022513>
- James R, Washington R, Schleussner CF, Rogelj J, Conway D (2017) Characterizing half-a-degree difference: a review of methods for identifying regional climate responses to global warming targets. *Wiley Interdiscip Rev Clim Change*. <https://doi.org/10.1002/wcc.457>
- James R, Washington R, Abiodun B, Kay G, Mutemi J, Pokam W, Hart N, Artan G, Senior C (2018) Evaluating climate models with an African lens. *Bull Am Meteorol Soc* 99(2):313–336. <https://doi.org/10.1175/BAMS-D-16-0090.1>
- Jones PW (1999) First-and second-order conservative remapping schemes for grids in spherical coordinates. *Mon Weather Rev* 127(9):2204–2210
- Jones CG, Willén U, Ullerstig A, Hansson U (2004) The Rossby Centre regional atmospheric climate model part I: model climatology and performance for the present climate over Europe. *AMBIO J Hum Environ* 33(4):199–210
- Jury MR, Matari E, Matitu M (2009) Equatorial African climate teleconnections. *Theor Appl Climatol* 95(3):407–416. <https://doi.org/10.1007/s00704-008-0018-4>
- Kain JS (2004) The Kain–Fritsch convective parameterization: an update. *J Appl Meteorol* 43(1):170–181
- Kalnay E, Kanamitsu M, Kistler R, Collins W, Deaven D, Gandin L, Iredell M, Saha S, White G, Woollen J, Zhu Y, Chelliah M, Ebisuzaki W, Higgins W, Janowiak J, Mo KC, Ropelewski C, Wang J, Leetmaa A, Reynolds R, Jenne R, Joseph D (1996) The NCEP/NCAR 40-year reanalysis project. *Bull Am Meteorol Soc* 77(3):437–472. [https://doi.org/10.1175/1520-0477\(1996\)077<0437:TNYRP>2.0.CO;2](https://doi.org/10.1175/1520-0477(1996)077<0437:TNYRP>2.0.CO;2)
- Kalognomou EA, Lennard C, Shongwe M, Pinto I, Favre A, Kent M, Hewitson B, Dosio A, Nikulin G, Panitz HJ, et al (2013) A diagnostic evaluation of precipitation in CORDEX models over southern Africa. *J Clim* 26(23):9477–9506. <https://doi.org/10.1175/JCLI-D-12-00703.1>
- Kanamitsu M, Ebisuzaki W, Woollen J, Yang SK, Hnilo JJ, Fiorino M, Potter GL (2002) Ncep?doe amip-ii reanalysis (r-2). *Bull Am Meteorol Soc* 83(11):1631–1644. <https://doi.org/10.1175/BAMS-83-11-1631>
- Kim J, Waliser DE, Mattmann CA, Goodale CE, Hart AF, Zimdars PA, Crichton DJ, Jones C, Nikulin G, Hewitson B, Jack C, Lennard C, Favre A (2014) Evaluation of the CORDEX-Africa multi-RCM hindcast: systematic model errors. *Clim Dyn* 42(5):1189–1202. <https://doi.org/10.1007/s00382-013-1751-7>
- King AD, Harrington LJ (2018) The inequality of climate change from 1.5oC to 2oC of global warming. *Geophys Res Lett*. <https://doi.org/10.1029/2018GL078430>
- Koster RD, Dirmeyer PA, Guo Z, Bonan G, Chan E, Cox P, Gordon CT, Kanae S, Kowalczyk E, Lawrence D, Liu P, Lu CH, Malyshov S, McAvaney B, Mitchell K, Mocko D, Oki T, Oleson K, Pitman A, Sud YC, Taylor CM, Verseghy D, Vasic R, Xue Y, Yamada T (2004) Regions of strong coupling between soil moisture and precipitation. *Science* 305(5687):1138–1140. <https://doi.org/10.1126/science.1100217>, <http://science.sciencemag.org/content/305/5687/1138>
- Laprise R (2008) Regional climate modelling. *J Comput Phys* 227(7):3641–3666. <https://doi.org/10.1016/j.jcp.2006.10.024>
- Laprise R, Hernández-Díaz L, Tete K, Sushama L, Šeparović L, Martynov A, Winger K, Valin M (2013) Climate projections over CORDEX Africa domain using the fifth-generation Canadian regional climate model (CRCM5). *Clim Dyn* 41(11):3219–3246. <https://doi.org/10.1007/s00382-012-1651-2>
- Lee JW, Hong SY (2014) Potential for added value to downscaled climate extremes over korea by increased resolution of a regional climate model. *Theor Appl Climatol* 117(3):667–677. <https://doi.org/10.1007/s00704-013-1034-6>
- Masson-Delmotte V, Zhai P, Pörtner HO, Roberts D, Skea J, Shukla P, Pirani A, Moufouma-Okia W, Péan C, Pidcock R, Connors S, Matthews JBR, Chen Y, Zhou X, Gomis MI, Lonnoy E, Maycock T, Tignor M, Waterfield Te (2018) Global warming of 1.5° c. an ipcc special report on the impacts of global warming of 1.5° c above pre-industrial levels and related global greenhouse gas emission pathways, in the context of strengthening the global response to the threat of climate change,

- sustainable development, and efforts to eradicate poverty. <https://www.ipcc.ch/sr15/> (in Press)
- Moufouma-Okia W, Jones R (2015) Resolution dependence in simulating the African hydroclimate with the HadGEM3-RA regional climate model. *Clim Dyn* 44(3):609–632. <https://doi.org/10.1007/s00382-014-2322-2>
- Muller CJ, Back LE, O’Gorman PA, Emanuel KA (2009) A model for the relationship between tropical precipitation and column water vapor. *Geophys Res Lett.* <https://doi.org/10.1029/2009GL039667>
- Neupane N (2016) The Congo Basin zonal overturning circulation. *Adv Atmos Sci* 33(6):767–782. <https://doi.org/10.1007/s00365-015-5190-8>
- Newell RE, Kidson JW, Vincent DG, Boer GJ (1972) The general circulation of the tropical atmosphere and interactions with extra-tropical latitudes, vol I. Massachusetts Institute of Technology, Boston, p 258
- Nicholson SE (2009) On the factors modulating the intensity of the tropical rainbelt over west Africa. *Int J Climatol J R Meteorol Soc* 29(5):673–689. <https://doi.org/10.1002/joc.1702>
- Nicholson SE (2018) The ITCZ and the seasonal cycle over equatorial Africa. *Bull Am Meteorol Soc* 99(2):337–348. <https://doi.org/10.1175/BAMS-D-16-0287.1>
- Nicholson SE, Grist JP (2003) The seasonal evolution of the atmospheric circulation over west Africa and equatorial Africa. *J Clim* 16(7):1013–1030. [https://doi.org/10.1175/1520-0442\(2003\)016<1013:TSEOTA>2.0.CO;2](https://doi.org/10.1175/1520-0442(2003)016<1013:TSEOTA>2.0.CO;2)
- Nikulin G, Jones C, Giorgi F, Asrar G, Büchner M, Cerezo-Mota R, Christensen OB, Déqué M, Fernandez J, Hänsler A et al (2012) Precipitation climatology in an ensemble of CORDEX-Africa regional climate simulations. *J Clim* 25(18):6057–6078. <https://doi.org/10.1175/JCLI-D-11-00375.1>
- Nikulin G, Lennard C, Dosio A, Kjellström E, Chen Y, Hänsler A, Kupiainen M, Laprise R, Mariotti L, Maule CF, van Meijgaard E, Panitz HJ, Scinocca JF, Somot S (2018) The effects of 1.5 and 2 degrees of global warming on Africa in the CORDEX ensemble. *Environ Res Lett* 13(6):065003. <http://stacks.iop.org/1748-9326/13/i=6/a=065003>
- Nishii K, Miyasaka T, Nakamura H, Kosaka Y, Yokoi S, Takayabu YN, Endo H, Ichikawa H, Inoue T, Oshima K et al (2012) Relationship of the reproducibility of multiple variables among global climate models. *J Meteorol Soc Jpn Ser II* 90:87–100. <https://doi.org/10.2151/jmsj.2012-A04>
- Noilhan J, Planton S (1989) A simple parameterization of land surface processes for meteorological models. *Mon Weather Rev* 117(3):536–549
- Paeth H, Mannig B (2013) On the added value of regional climate modeling in climate change assessment. *Clim Dyn* 41(3):1057–1066. <https://doi.org/10.1007/s00382-012-1517-7>
- Panitz HJ, Dosio A, Büchner M, Lüthi D, Keuler K (2014) COSMO-CLM (CCLM) climate simulations over CORDEX-Africa domain: analysis of the ERA-interim driven simulations at 0.44 degree and 0.22 degree resolution. *Clim Dyn* 42(11):3015–3038. <https://doi.org/10.1007/s00382-013-1834-5>
- Pokam WM, Djotang LAT, Mkankam FK (2012) Atmospheric water vapor transport and recycling in equatorial central Africa through NCEP/NCAR reanalysis data. *Clim Dyn* 38(9–10):1715–1729. <https://doi.org/10.1007/s00382-011-1242-7>
- Pokam WM, Bain CL, Chadwick RS, Graham R, Sonwa DJ, Kamga FM (2014) Identification of processes driving low-level westerlies in west equatorial Africa. *J Clim* 27(11):4245–4262. <https://doi.org/10.1175/JCLI-D-13-00490.1>
- Pokam WM, Longandjo GNT, Moufouma-Okia W, Bell JP, James R, Vondou DA, Haensler A, Fotso-Nguemo TC, Guenang GM, Tchotchou ALD, Kamsu-Tamo PH, Takong RR, Nikulin G, Lennard CJ, Dosio A (2018) Consequences of 1.5° c and 2° c global warming levels for temperature and precipitation changes over central Africa. *Environ Res Lett* 13(5):055011. <http://stacks.iop.org/1748-9326/13/i=5/a=055011>
- Popke D, Stevens B, Voigt A (2013) Climate and climate change in a radiative–convective equilibrium version of ECHAM6. *J Adv Model Earth Syst* 5(1):1–14. <https://doi.org/10.1029/2012GM000191>
- Qin D, Plattner G, Tignor M, Allen S, Boschung J, Nauels A, Xia Y, Bex V, Midgley P, et al (2013) Summary for policymakers. In: Stocker TF et al (eds) Climate change 2013: the physical science basis contribution of working group I to the fifth assessment report of the intergovernmental panel on climate change. Contribution of working group I to the Fifth assessment report of the intergovernmental panel on climate change, pp 5–14
- Räisänen P, Rummukainen M, Räisänen J (2000) Modification of the HIRLAM radiation scheme for use in the Rossby Centre regional atmospheric climate model. Department of Meteorology, University of Helsinki, Helsinki
- Riahi K, Rao S, Krey V, Cheolhung CC, Chirkov V, Fischer G, Kindermann G, Nakicenovic N, Rafaj P (2011) RCP 8.5—a scenario of comparatively high greenhouse gas emissions. *Clim Change* 109:33–57. <https://doi.org/10.1007/s10584-011-0149-y>
- Roehrig R, Bouniol D, Guichard F, Hourdin F, Redelsperger JL (2013) The present and future of the West African monsoon: a process-oriented assessment of CMIP5 simulations along the AMMA transect. *J Clim* 26(17):6471–6505. <https://doi.org/10.1175/JCLI-D-12-00505.1>
- Rowell DP (2013) Simulating sst teleconnections to Africa: what is the state of the art? *J Clim* 26(15):5397–5418. <https://doi.org/10.1175/JCLI-D-12-00761.1>
- Rowell DP, Senior CA, Vellinga M, Graham RJ (2016) Can climate projection uncertainty be constrained over Africa using metrics of contemporary performance? *Clim Change* 134(4):621–633. <https://doi.org/10.1007/s10584-015-1554-4>
- Samuelsson P, Jones CG, Willén U, Ullerstig A, Gollvik S, Hansson U, Jansson C, Kjellström E, Nikulin G, Wyser K (2011) The Rossby Centre regional climate model RCA3: model description and performance. *Tellus A* 63(1):4–23
- Samuelsson P, Gollvik S, Kupiainen M, Kourzeneva E, van de Berg WJ (2015) The surface processes of the Rossby Centre regional atmospheric climate model (RCA4). Technical report 157, Climate research-Rossby Centre
- Sass B, Rontu L, Räisänen P (1994) HIRLAM-2 radiation scheme: documentation and tests. HIRLAM technical report, vol 16. HIRLAM 3 Project, Swed. Meteorolog. and Hydrolog. Inst., <https://books.google.cm/books?id=GS5YnQAACAAJ>
- Savijärvi H (1990) Fast radiation parameterization schemes for mesoscale and short-range forecast models. *J Appl Meteorol* 29(6):437–447
- Schneider AFPMCARBZM Udo; Becker (2011) Gpcc full data reanalysis version 7.0 at 0.5 degree: monthly land-surface precipitation from rain-gauges built on gtsbased and historic data. Global Precipitation Climatology Centre (GPCC), DWD 112. https://doi.org/10.5676/DWD_GPCC_FD_M_V6_05
- Seneviratne SI, Viterbo P, Lüthi D, Schaer C (2004) Inferring changes in terrestrial water storage using ERA-40 reanalysis data: the Mississippi River basin. *J Clim* 17(11):2039–2057. [https://doi.org/10.1175/1520-0442\(2004\)017<2039:ICITWS>2.0.CO;2](https://doi.org/10.1175/1520-0442(2004)017<2039:ICITWS>2.0.CO;2)
- Shi F, Hao Z, Shao Q (2014) The analysis of water vapor budget and its future change in the Yellow-huai-hai region of China. *J Geophys Res Atmos.* <https://doi.org/10.1002/2013JD021431>
- Sonkoué D, Monkam D, Fotso-Nguemo TC, Yepdo ZD, Vondou DA (2018) Evaluation and projected changes in daily rainfall characteristics over central Africa based on a multi-model ensemble mean of CMIP5 simulations. *Theor Appl Climatol.* <https://doi.org/10.1007/s00704-018-2729-5>

- Strandberg G, Bärring L, Hansson U, Jansson C, Jones C, Kjellström E, Kupiainen M, Nikulin G, Samuelsson P, Ullerstig A (2015) CORDEX scenarios for Europe from the Rossby Centre regional climate model RCA4. Technical report 116, Climate research-Rossby Centre
- Sun B, Wang H (2018a) Enhanced connections between summer precipitation over the three-river-source region of China and the global climate system. *Clim Dyn*. <https://doi.org/10.1007/s00382-018-4326-9>
- Sun B, Wang H (2018b) Interannual variation of the spring and summer precipitation over the three river source region in China and the associated regimes. *J Clim* 31(18):7441–7457. <https://doi.org/10.1175/JCLI-D-17-0680.1>
- Tamoffo AT, Vondou DA, Pokam WM, Haensler A, Yedo ZD, Fotso-Nguemo TC, Tchotchou LAD, Nouayou R (2019) Daily characteristics of central African rainfall in the REMO model. *Theor Appl Climatol*. <https://doi.org/10.1007/s00704-018-2745-5>
- Taylor KE, Stouffer RJ, Meehl GA (2012) An overview of CMIP5 and the experiment design. *Bull Am Meteorol Soc* 93(4):485. <https://doi.org/10.1175/BAMS-D-11-00094.1>
- Tchotchou LAD, Kamga FM (2010) Sensitivity of the simulated African monsoon of summers 1993 and 1999 to convective parameterization schemes in RegCM3. *Theor Appl Climatol* 100(1):207–220. <https://doi.org/10.1007/s00704-009-0181-2>
- Teichmann C, Bülow K, Otto J, Pfeifer S, Rechid D, Sieck K, Jacob D (2018) Avoiding extremes: benefits of staying below +1.5° c compared to +2.0° c and +3.0° c global warming. *Atmosphere*. <https://doi.org/10.3390/atmos904115>. <http://www.mdpi.com/2073-4433/9/4/115>
- Thomson AM, Calvin KV, Smith SJ, Kyle GP, Volke A, Patel P, Delgado-Arias S, Bond-Lamberty B, Wise MA, Clarke LE, Edmonds JA (2011) RCP4.5: a pathway for stabilization of radiative forcing by 2100. *Clim Change* 109(1):77. <https://doi.org/10.1007/s10584-011-0151-4>
- Tokinaga H, Xie SP, Timmermann A, McGregor S, Ogata T, Kubota H, Okumura YM (2012) Regional patterns of tropical Indo-pacific climate change: evidence of the Walker circulation weakening. *J Clim* 25(5):1689–1710. <https://doi.org/10.1175/JCLI-D-11-00263.1>
- Trenberth KE (1999) Atmospheric moisture recycling: role of advection and local evaporation. *J Clim* 12(5):1368–1381. [https://doi.org/10.1175/1520-0442\(1999\)012<1368:AMRROA>2.0.CO;2](https://doi.org/10.1175/1520-0442(1999)012<1368:AMRROA>2.0.CO;2)
- Unden P, Rontu L, Jinen H, Lynch P, Calvo J, Cats G, Cuxart J, Eerola K, Fortelius C, Garcia-Moya JA, Jones C, Geert, Lenderlink G, McDonald A, McGrath R, Navascues B, Nielsen NW, Degaard V, Rodriguez E, Rummukainen M, Sattler K, Sass BH, Savijarvi H, Schreier BW, Sigg R, The H (2002) Hirlam-5 scientific documentation. http://www.knmi.nl/hirlam/SciDoc_Dec2002.pdf
- Van der Ent RJ, Savenije HH (2013) Oceanic sources of continental precipitation and the correlation with sea surface temperature. *Water Resour Res* 49(7):3993–4004. <https://doi.org/10.1002/wrcr.20296>
- Van der Ent RJ, Savenije HH, Schaefli B, Steele-Dunne SC (2010) Origin and fate of atmospheric moisture over continents. *Water Resour Res*. <https://doi.org/10.1029/2010WR009127>
- Voldoire A, Sanchez-Gomez E, Salas y Méria D, Decharme B, Cassou C, Sénési S, Valcke S, Beau I, Alias A, Chevallier M, Déqué M, Deshayes J, Douville H, Fernandez E, Madec G, Maisonneuve E, Moine MP, Planton S, Saint-Martin D, Szopa S, Tytقة S, Alkama R, Belamari S, Braun A, Coquart L, Chauvin F (2013) The CNRM-CM5.1 global climate model: description and basic evaluation. *ClimDyn* 40(9):2091–2121. <https://doi.org/10.1007/s00382-011-1259-y>
- Vondou DA, Haensler A (2017) Evaluation of simulations with the regional climate model REMO over central Africa and the effect of increased spatial resolution. *Int J Climatol* 37:741–760. <https://doi.org/10.1002/joc.5035>
- Washington R, James R, Pearce H, Pokam WM, Moufouma-Okia W (2013) Congo basin rainfall climatology: can we believe the climate models? *Philos Trans R Soc Lond B Biol Sci*. <https://doi.org/10.1098/rstb.2012.0296>. <http://rstb.royalsocietypublishing.org/content/368/1625/20120296>
- Watanabe S, Hajima T, Sudo K, Nagashima T, Takemura T, Okajima H, Nozawa T, Kawase H, Abe M, Yokohata T, et al. (2011) Miroc-esm 2010: model description and basic results of cmip5-20c3m experiments. *Geosci Model Dev Discuss* 4:1063–1128. <https://doi.org/10.5194/gmd-4-1063-2011>
- Watterson I, Bathols J, Heady C (2014) What influences the skill of climate models over the continents? *Bull Am Meteorol Soc* 95(5):689–700. <https://doi.org/10.1175/BAMS-D-12-00136.1>
- Weber T, Haensler A, Rechid D, Pfeifer S, Eggert B, Jacob D (2018) Analyzing regional climate change in Africa in a 1.5, 2, and 3 c global warming world. *Earth's Future* 6(4):643–655. <https://doi.org/10.1002/2017EF000714>
- Williams CA, Hanan NP, Neff JC, Scholes RJ, Berry JA, Denning AS, Baker DF (2007) Africa and the global carbon cycle. *Carbon Balance Manag* 2(1):3. <https://doi.org/10.1186/1750-0680-2-3>
- Xie P, Arkin PA (1997) Global precipitation: a 17-year monthly analysis based on gauge observations, satellite estimates, and numerical model outputs. *Bull Am Meteorol Soc* 78(11):2539–2558. [https://doi.org/10.1175/1520-0477\(1997\)078<2539:GPAYM_A>2.0.CO;2](https://doi.org/10.1175/1520-0477(1997)078<2539:GPAYM_A>2.0.CO;2)
- Yin L, Fu R, Shevliakova E, Dickinson RE (2013) How well can CMIP5 simulate precipitation and its controlling processes over tropical South America? *Clim Dyn* 41(11):3127–3143. <https://doi.org/10.1007/s00382-012-1582-y>
- Zhang Q, Körnich H, Holmgren K (2013) How well do reanalyses represent the southern African precipitation? *Clim Dyn* 40(3):951–962. <https://doi.org/10.1007/s00382-012-1423-z>
- Zheng X, Eltahir EA (1998) The role of vegetation in the dynamics of west African monsoons. *J Clim* 11(8):2078–2096. <https://doi.org/10.1175/1520-0442>

Affiliations

Alain T. Tamoffo^{1,2}  · Wilfran Moufouma-Okia³  · Alessandro Dosio⁴  · Rachel James⁵  · Wilfried M. Pokam^{1,2,6}  · Derbetini A. Vondou^{1,2}  · Thierry C. Fotso-Nguemo^{1,7}  · Guy Merlin Guenang^{1,8}  · Pierre H. Kamsu-Tamo^{1,9,10}  · Grigory Nikulin¹¹  · Georges-Noel Longandjo¹²  · Christopher J. Lennard¹³  · Jean-Pierre Bell¹⁴  · Roland R. Takong¹³  · Andreas Haensler¹⁵  · Lucie A. Djotang Tchotchou¹  · Robert Nouayou¹⁶ 

¹ Laboratory for Environmental Modelling and Atmospheric Physics (LEMAP), Department of Physics, University of Yaounde 1, P.O. Box 812, Yaounde, Cameroon

² 2LMI DYCOFAC (IRD, University of Yaounde 1, IRGM), IRD, BP1857, Yaoundé, Cameroun

- ³ Université Paris Saclay, Intergovernmental Panel on Climate Change (IPCC) Working Group 1 (WG1) Technical Support Unit (TSU), Saint Aubin, France
- ⁴ European Commission, Joint Research Centre (JRC), Ispra, Italy
- ⁵ Environmental Change Institute, University of Oxford, Oxford, UK
- ⁶ Department of Physics, Higher Teacher Training College, University of Yaounde 1, P.O. Box 47, Yaounde, Cameroon
- ⁷ Climate Change Research Laboratory (CCRL), National Institute of Cartography, P.O. Box 157, Yaounde, Cameroon
- ⁸ Laboratory of Mechanics and Modeling of Physical Systems, Department of Physics, Faculty of Science, University of Dschang, Po Box 67, Dschang, Cameroon
- ⁹ Climate Prediction Center, National Centers for Environmental Predictions, National Oceanic and Atmospheric Administration, College Park, MD, USA
- ¹⁰ Cooperative Programs for the Advancement of Earth System Science, University Corporation for Atmospheric Research, Boulder, CO, USA
- ¹¹ Rossby Centre, Swedish Meteorological and Hydrological Institute, Norrköping, Sweden
- ¹² Department of Oceanography, Nansen-Tutu Center for Environmental Marine Research, University of Cape Town, Cape Town, South Africa
- ¹³ Department of Environmental and Geographical Science, University of Cape Town, Cape Town, South Africa
- ¹⁴ CEPAMOQ, Faculty of Science, University of Douala, Douala, Cameroon
- ¹⁵ Helmholtz-Zentrum Geesthacht, Climate Service Center Germany, Hamburg, Germany
- ¹⁶ Laboratory of Geophysics and Geoexploration, Department of Physics, University of Yaounde 1, P.O. Box 812, Yaounde, Cameroon